CELL BIOLOGY

Inflammatory monocytes constrain YAP-induced cell proliferation

Serrena Singh[1,2], Nareh Tahmasian[3], Jia-Jun Liu[4], Wenjia Wang[4], Lucas Haas[1,2], Yingdong Zhu[1,2], Magdalena M. Griswold[5], Nina N. Brodsky[5], Silvia Liu[4], Brian T. Kalish[3,6,7,8], Dean Yimlamai[1,2]*

***YAP* and its paralog, *TAZ*, are transcriptional coactivators of the Hippo pathway that regulate cell growth. Their structural distinctiveness suggests important independent functional differences. To investigate this further, we generated YAP- and TAZ-predominant clones in the liver and followed their long-term behavior. YAP clones rapidly dedifferentiate cells into a stem cell–like state with inflammatory immune cell recruitment followed by their clearance. In contrast, TAZ clones promote an anti-inflammatory immune environment, resulting in their long-term maintenance, massive organ growth, and increased mortality. YAP clones recruit inflammatory blood-derived monocytes, which, if inhibited, permits YAP clonal growth. Consistent with these results, patients with *YAP*^{High} colorectal cancer (CRC) had a 67% 5-year survival rate, whereas patients with *TAZ*^{High} CRC did not survive to 5 years. Similar trends were seen in patients with hepatocellular carcinoma. These findings underscore the importance of understanding the intrinsic differences in YAP and TAZ biology as independent drivers of disease.**

INTRODUCTION

Genetic duplication is useful for the long-term survival of a species, ensuring redundancy of useful traits as well as providing the starting material for genetic diversity through processes like neofunctionalization (*1*, *2*). Over time, duplicated genes undergo mutations, leading to their divergence to develop new functions. In vertebrates, the transcriptional coactivators Yes1-associated protein (*YAP*) and its paralog WW domain containing transcriptional regulator (*WWTR1*, aka *TAZ*) are one example of this process.

Both *YAP* and *TAZ* are thought to arise from the same ancestral gene, *yorkie* (*yki*) (*3*). *Yki*, originally discovered in *Drosophila* integrates intra/extracellular cues regulating programs involved in cell proliferation, differentiation, and stem cell renewal within a highly conserved framework known as the Hippo signaling pathway (*4*–*7*). *Yorkie* and other critical Hippo pathway components are present in unicellular premetazoan lineages (*8*–*10*) with the gene duplication event producing *YAP* and *TAZ* occurring in an early vertebrate ancestor (*11*).

YAP and *TAZ* are often referred interchangeably, likely because early studies focused on their involvement in proliferation (*12*). Studies defining differences between *YAP* and *TAZ* are comparatively sparse with apparent differences in their biology often hypothesized to primarily be due to their genomic regulation (*10*). Vertebrates have adopted an increasing number of inputs into these molecules, but whether or how *YAP*/*TAZ* translates these signals into differential outputs requiring the presence of two distinctive cotransactivators is unclear.

Several similarities and distinctions between these proteins exist. They share the ability to interact and activate the TEA Domain (TEAD) family of transcription factors (*13*) and appear to respond similarly to upstream kinases (*14*). But, YAP is significantly larger than TAZ, with YAP containing several phosphorylation sites and domains absent from TAZ. TAZ has an ability to homodimerize while YAP does not, suggesting that these molecules can form distinct intracellular binding partners to activate/inhibit divergent downstream transcriptional targets (*15*, *16*).

Here, we investigated the role that these molecules play by manipulating YAP or TAZ expression in hepatocytes. Both YAP and TAZ support an initial burst of proliferative activity by hepatocytes. Over time, TAZ-expressing hepatocytes rapidly overtake the liver parenchyma, whereas YAP-expressing hepatocytes remain limited in their growth. We find that YAP-expressing hepatocytes illicit a strong immunologic response, recruiting monocytes and other innate immune cells which limit YAP clonal growth. In contrast, TAZ-expressing hepatocytes display fewer immunostimulatory signaling pathways, thereby fostering their long-term growth. In colorectal cancer (CRC) and hepatocellular carcinoma (HCC), high TAZ expression was associated with a shorter survival time than those expressing high YAP.

RESULTS

LATS KO cells in vivo predominantly express TAZ expression and display a competitive growth advantage over YAP

To examine the effects of YAP versus TAZ on in vivo cellular behavior, we generated two mouse lines for comparison. First, we used a previously published tetracycline-inducible model of *YAPS127A* (Fig. 1A, YAP-Tg) (*17*) that is paired with a constitutive reverse tetracycline transactivator blocked by a floxed stop cassette (*18*). Mice are infected with a highly specific adeno-associated virus specifically expressed in hepatocytes (AAV-Cre). Doxycyline is then given in the drinking water to activate *YAP* expression in a cell-type and temporal specific fashion.

[1]Section of Pediatric Gastroenterology, Hepatology, and Nutrition, Yale School of Medicine, New Haven, CT 06520, USA. [2]Yale Liver Center, Department of Medicine, Yale School of Medicine, New Haven, CT 06520, USA. [3]Program in Neuroscience and Mental Health, SickKids Research Institute, Toronto, ON M5G 1L7, Canada. [4]Organ Pathobiology and Therapeutics Institute, Department of Pharmacology and Chemical Biology, Pittsburgh Liver Research Center, University of Pittsburgh School of Medicine, Pittsburgh, PA 15261, USA. [5]Section of Critical Care Medicine, Department of Pediatrics, Yale School of Medicine; New Haven, CT 06520, USA. [6]Department of Molecular Genetics, University of Toronto, Toronto, ON M5G 1A8, Canada. [7]Division of Neonatology, Department of Paediatrics, Hospital for Sick Children, Toronto, ON, Canada. [8]Division of Neonatology, Department of Pediatrics, Boston Children's Hospital, Boston 02115, MA, USA.
*Corresponding author. Email: dean.yimlamai@yale.edu

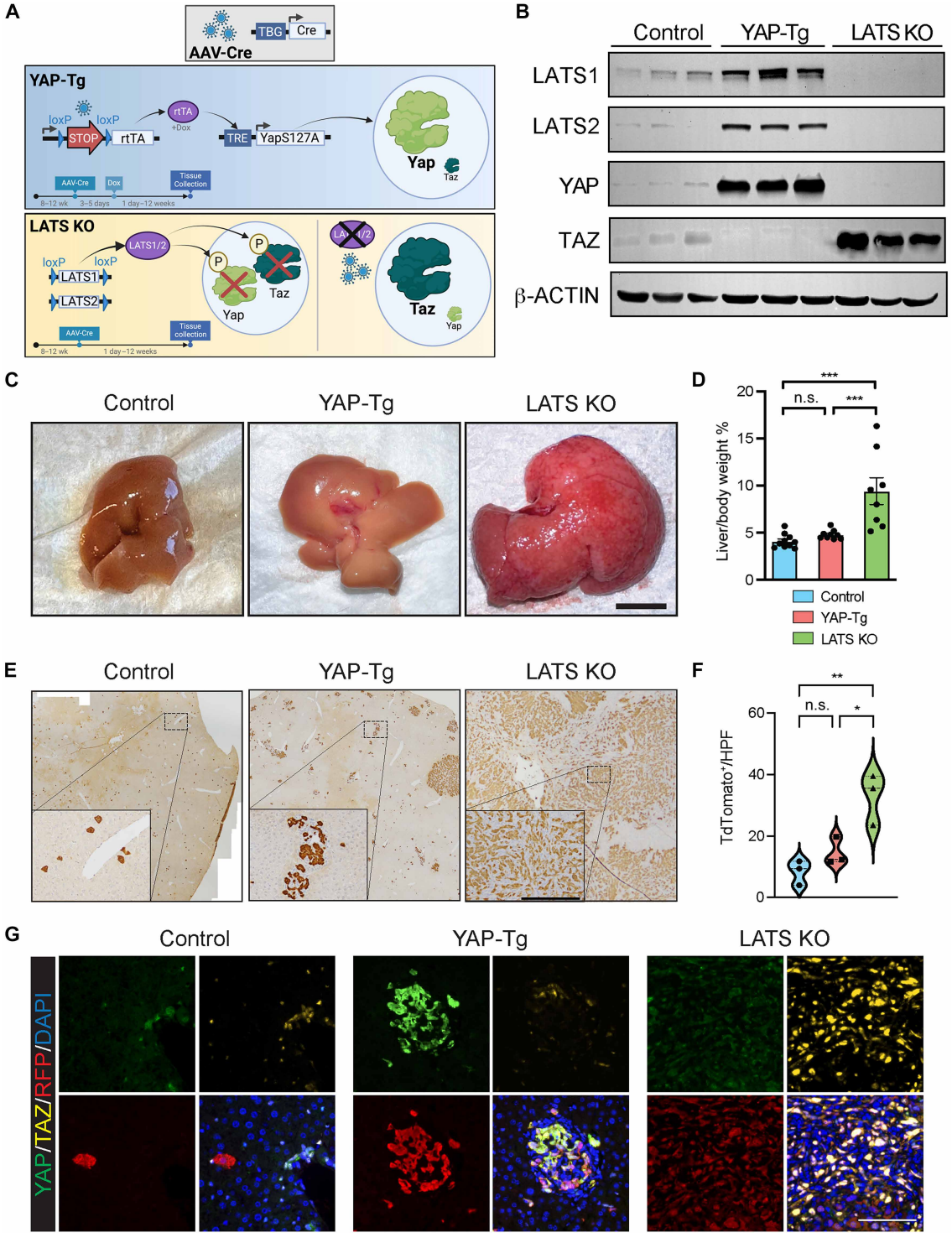

Fig. 1. Hepatocyte-specific LATS KO confers growth advantage as compared to YAP-Tg. (**A**) Schematic of experimental setup and model design. Created in BioRender. D. Yimlamai (2026), https://BioRender.com/6l1npfn. wk, weeks. (**B**) Western blot of livers from control, YAP-Tg, and LATS KO mice at 3 weeks post–AAV-Cre [10^{11} plaque-forming units (PFU) per mouse] and doxycycline water administration with the indicated antibodies. (**C**) Representative images of control, YAP-Tg, and LATS KO livers harvested 12 weeks postinduction with AAV-Cre (10^9 PFU per mouse). Scale bar, 1 cm. (**D**) Bar plot of liver/body weight percentages in control ($n = 10$), YAP-Tg ($n = 9$), and LATS KO mice ($n = 8$). (**E**) Representative tdTomato immunostaining of cells in control, YAP-Tg, and LATS KO mice. Inset: Magnified image of indicated area. Scale bar, 200 μm. (**F**) Violin plot of TdTomato$^+$ cells per high-power field (HPF) for conditions noted in (E) ($n = 3$ animals per group; Tukey's multiple comparisons test). (**G**) Representative images of immunostaining of YAP (green), TAZ (yellow), red fluorescent protein (RFP; red), and 4′,6-diamidino-2-phenylindole (DAPI; blue) in the indicated livers. Scale bar, 90 μm. Mean and SEM plotted; *P* value calculated with one-way analysis of variance (ANOVA), Tukey's multiple comparisons test. n.s., not significant; $^*P < 0.05$; $^{**}P < 0.01$; $^{***}P < 0.001$. AAV-Cre, AAV-TBG-Cre; Dox, doxycycline.

Second, we generated Large Tumor Suppressor kinase 1 and 2 (*LATS1/2*) knockout (KO) mice by infecting *LATS1/2* floxed mice with AAV-Cre (Fig. 1A, LATS KO). LATS kinases (*LATS1* and *LATS2*) are well-established upstream regulators of YAP and TAZ (*19*–*22*), phosphorylating these proteins to promote their cytoplasmic sequestration and degradation. Previous studies using similar methods suggested that *LATS1/2* deletion leads to up-regulation of both YAP and TAZ (*23*–*25*).

A time-course study of YAP-Tg and LATS KO mice was performed to document the dynamics of YAP and TAZ expression in vivo. At all time points examined, YAP-Tg mice predominantly expressed YAP and minimal TAZ. In LATS KO mice 1 week after infection, there was broad hepatocytic nuclear YAP expression and minimal TAZ expression. At 2 weeks, proliferative clones displayed a combination of nuclear YAP and TAZ expression, whereas, at 3 weeks, expanding clones predominantly expressed nuclear TAZ and minimal YAP expression (fig. S1A). Liver immunoblots at this time point showed that control livers (AAV-Cre/R26-lsl-tdTomato) demonstrated modest expression of YAP and TAZ. YAP-Tg livers demonstrated high YAP expression and reciprocally low TAZ expression. Consistent with the immunostaining results, LATS KO livers demonstrated high TAZ expression and correspondingly low YAP expression (Fig. 1B).

We then evaluated whether persistent activation of YAP or TAZ in a small number of hepatocytes results in measurable long-term differences in liver size or animal health. Using a low dose of AAV-Cre to infect a small number of hepatocytes (~0.1%), we followed a cohort of mice over a 12-week treatment period. An inducible tandem-dimer tomato (tdTomato) reporter present in these lines facilitates clonal tracing of recombined cells. LATS KO animals had early mortality and lower survival rates (8 of 11) compared to control (10 of 10) and YAP-Tg (9 of 10) animals, suggesting a potential disparity across the models (fig. S1B, $P = 0.08$). When the livers were harvested, we observed that LATS KO livers were markedly larger (9.4%, $n = 8$, $P < 0.001$; Fig. 1, C and D) with pronounced redness as compared to either of the control or YAP-Tg groups. Control and YAP-Tg livers were tan in appearance with similar mean liver–to–body weight ratios for control (4.1%, $n = 10$) and YAP-Tg (4.8%, $n = 9$) mice (Fig. 1, C and D). These values fall well within the normal range for normal mice (3 to 5%).

To discern the cellular behavior of hepatocytes in the context of YAP or TAZ overexpression, we microscopically examined representative livers from these treatments. tdTomato$^+$ cells in control livers were typically single cells, consistent with the notion that hepatocytes divide once or twice per year under homeostasis (*26*). In YAP-Tg livers, we observed both single cells and small heterogeneous clusters scattered throughout the liver. This is consistent with prior work demonstrating that YAP overexpression plays a role stimulating hepatocyte growth, although not to an extent where it was macroscopically visible in this setting. In contrast, LATS KO mice had small tdTomato$^+$ cells throughout the liver parenchyma (Fig. 1E). Individual clones were indistinguishable in the LATS KO model, presumably because clones merged with one another.

We quantified the number of tdTomato$^+$ cells per high-power field (HPF) to measure the persistence of recombined cells 12 weeks after each treatment. Control, YAP-Tg, and LATS KO livers displayed 10.1, 12.9, and 32.4 tdTomato$^+$ cells per HPF, respectively (Fig. 1F). Immunohistochemistry showed that tdTomato$^+$ cells in controls did not express substantial amounts of either YAP or TAZ. tdTomato$^+$ clones in YAP-Tg and LATS KO livers predominantly expressed either YAP or TAZ, respectively (Fig. 1G and fig. S1, C and D). These findings indicate that both YAP and TAZ stimulate clonal growth; however, TAZ^{High} hepatocytes display a substantial growth advantage over YAP^{High} hepatocytes in vivo.

YAP-Tg and LATS KO hepatocytes share many common but some distinct transcriptional programs

To elucidate the transcriptional programs stimulated by YAP- or TAZ-predominant cells and gain insight into the differential mechanisms by which they expand in the liver, we performed bulk RNA sequencing (RNA-seq) on purified hepatocytes from control, YAP-Tg, and LATS KO livers (Fig. 2A). Three weeks posttreatment, we sorted hepatocytes from the liver by enzymatic digestion and purifying Live$^+$tdTomato$^+$ cells by fluorescence-activated cell sorting (FACS). Bulk RNA-seq libraries were generated and analyzed from these mice using stringent criteria (log fold change > 1.5, q value < 0.001; Fig. 2B). By this method, we identified common (104 genes, 35.6%), YAP-Tg (172 genes, 58.9), and LATS KO (15 genes, 5.1%) that were most likely to be commonly or uniquely expressed to these treatments.

Among the differentially expressed genes in YAP-Tg/LATS KO livers as compared to control were many well-documented Hippo pathway target genes (Fig. 2C, common) including *Ctgf*, *Cyr61*, *Nuak2*, and *Tgfb2*. In our common gene set, we identified *Anln* and *Kif23* as up-regulated, genes recently reported as key TAZ-specific target genes (*27*). LATS KO hepatocytes expressed *Ctla4* and *Tigit* (Fig. 2C, LATS KO specific), genes associated with promoting immune silencing by down-regulation of CD8$^+$ T cells (*28*). In contrast, YAP-Tg hepatocytes expressed several genes associated with interferon signaling activation including *Irf9*, *Isg15*, and *Igtp* (Fig. 2C, YAP-Tg specific).

To determine whether specific gene programs are preferentially activated in YAP-Tg or LATS KO livers, we used ingenuity pathway analysis (IPA). The analysis revealed several signaling pathways related to interferon and cell death activation pathways that were more strongly associated with YAP-Tg as compared to LATS KO (Fig. 2D). Notable among these were RIPK1-mediated necrosis, necroptosis signaling pathway, and interferon signaling. These pathways suggest a heightened inflammatory environment and potential cell death mechanisms linked to YAP-Tg expression. Conversely, the analysis of LATS KO livers revealed an enrichment of interleukin-10 signaling, an anti-inflammatory pathway associated with down-regulation of immune responses (*29*, *30*).

To confirm our findings, we examined an independent RNA-seq dataset using sorted hepatocytes from liver YAP overexpression (ApoE-YAP) (*31*) and LATS KO 1 week postinduction (*25*). Using similar criteria to our RNA-seq analysis, we identified a comparable proportion of genes grouping into common, ApoE-YAP–, and LATS KO–specific categories (fig. S2A) as in our dataset. IPA of this dataset revealed that the ApoE-YAP model was enriched for pathways associated with cell clearance and immune stimulation. In contrast, LATS KO livers displayed enrichment for pathways related to immune silencing (fig. S2, B and C). Together, these data suggest that YAP- and TAZ-predominant cells direct distinctive patterns of expression. YAP-Tg–expressing cells display genes associated with increased recruitment and activation of innate and adaptive immune cells, suggesting a robust immune response that potentially could slow their growth (*32*–*37*), while LATS KO cells express genes associated with immune silencing.

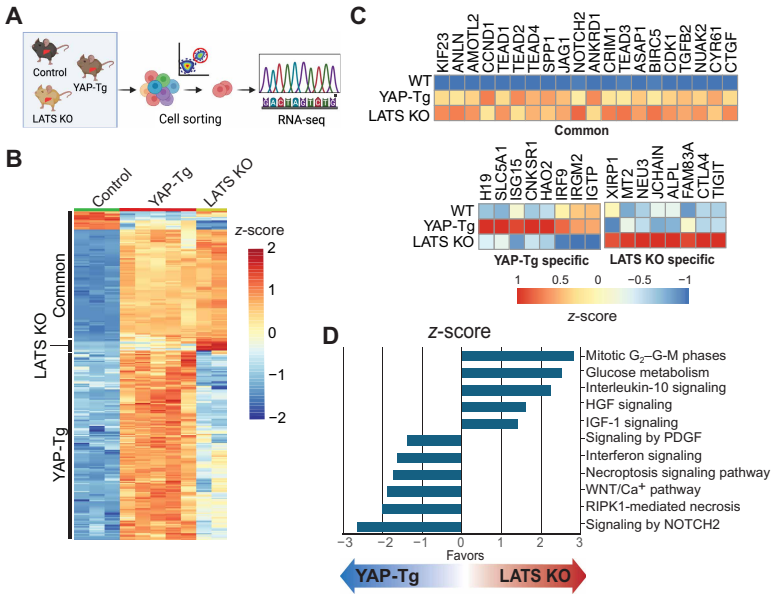

Fig. 2. Transcriptional profiling of YAP-Tg and LATS KO hepatocytes reveal transcripts and transcriptional profile favoring YAP or TAZ expression. (**A**) tdTomato-labeled cells of livers were cell sorted and subject to RNA-seq. Created in BioRender. D. Yimlamai (2026), https://BioRender.com/4ix922h. (**B**) Heatmap of control, LATS KO, and YAP-Tg hepatocytes. Common, YAP-Tg–, or LATS KO–specific transcripts are defined as less or greater than 1.5-log fold change and q value < 0.001. (**C**) Relative expression of common, YAP-Tg–, or LATS KO–specific genes from the indicated treatments. (**D**) Ingenuity pathway analysis (IPA) z-score associated with YAP or LATS KO. Analysis was performed on genes identified as significantly differently expressed based on the cutoffs reported in (B). HGF, hepatocyte growth factor; IGF-1, insulin-like growth factor 1; PDGF, platelet-derived growth factor; RIPK1, receptor-interacting protein kinase 1.

YAP-Tg and LATS KO single-nucleus RNA-seq uncovers distinctive patterns of cellular remodeling

To gain a deeper insight into the cellular behaviors that develop in YAP-Tg and LATS KO mice, we performed single-nucleus RNA-seq (snRNA-seq) on liver samples from control ($n = 2$), LATS KO ($n = 4$), and YAP-Tg mice ($n = 5$) (Fig. 3A). A total of 45,739 nuclei were recovered identifying 12 major clusters (Fig. 3B). Among these nuclei, we distinguished key liver cell populations, including cholangiocytes, hepatocytes, endothelial cells, fibroblasts, and immune cells. We were able to define the three major categories of hepatocytes—periportal, midzonal, and pericentral—by the expression of several well-known marker genes (Fig. 3B and fig. S3A). We classified a small subset of cells, "hepatic stem cells" due to their expression of cholangiocyte and periportal hepatocyte genes, a likely transitional population between the major epithelial cells of the liver. In controls, these cells represented 5.1% of all cells identified (Fig. 3, B to D, and table S1).

Activation of hepatocytic YAP results in profound changes in the proportion of epithelial and immune cells of the liver. The number and proportion of hepatic stem cells in YAP-Tg mice increased (22.9%) with a concomitant decrease in the proportion of cells identified as periportal hepatocytes (13.5%) as compared to controls (47.4%). In YAP-Tg mice, we identified a novel cellular population that we designated, "induced hepatic stem cells" (iHepSCs; 3.1%). These cells were not present in controls and shared characteristics of cholangiocytes and hepatic stem cells. These cells were highly proliferative as evidenced by expression of *Mki67* and exhibited markers of liver cancer stemness such as *Foxm1* (fig. S3A) (*38*). The proportion of cholangiocytes also markedly increased in the YAP-Tg model (18.7%) as compared to controls (2%). In comparison, the proportion of epithelial cells in control and LATS KO livers is highly similar (Fig. 3D). iHepSCs were present in LATS KO livers (0.5%), but they composed a small proportion of these livers and were several-fold lower than in the YAP-Tg model.

To further investigate how YAP or TAZ influences hepatocyte cell fate decisions, we applied Monocle3 trajectory analysis (*39*, *40*) to our parenchymal snRNA-seq dataset, ordering cells along a pseudotime axis. In control livers, most parenchymal cells were committed to the hepatocyte lineage with a small fraction transitioning between hepatocyte and cholangiocyte fates. YAP-Tg livers demonstrated a strong preference for hepatocytes to transition into cholangiocytes, hepatic stem cells, and iHepSCs and away from the periportal hepatocyte phenotype. In contrast, hepatocytes in LATS KO livers displayed cellular trajectories like the control condition (Fig. 3E). These findings underscore YAP's tendency to drive hepatocytes toward a progenitor-like state, a phenomenon not mirrored by TAZ expression.

There were notable shifts in the nonparenchymal cell populations of the YAP-Tg and LATS KO livers as compared to controls, particularly the immune cell fraction. Immune cells were 17.6 and 14.7% of YAP-Tg and LATS KO livers, respectively, whereas controls displayed 10% (Fig. 3C). By immunofluorescence, YAP-Tg (48.9 $CD45^+$ cells per HPF, $P < 0.0001$) had the highest proportion of immune cell recruitment followed by LATS KO (26.7 $CD45^+$ cells per HPF, $P < 0.001$) and then controls (10.4 $CD45^+$ cells per HPF; fig. S3, C and D). This change was also reflected when subclustering for *Ptprc* (i.e., *CD45*) expressing cells from our dataset. We identified several common immune cell types (fig. S3, B and E) such as Kupffer cells (KCs), macrophages, monocytes, dendritic cells, and B and T cells according to commonly expressed immune marker genes (*41*, *42*).

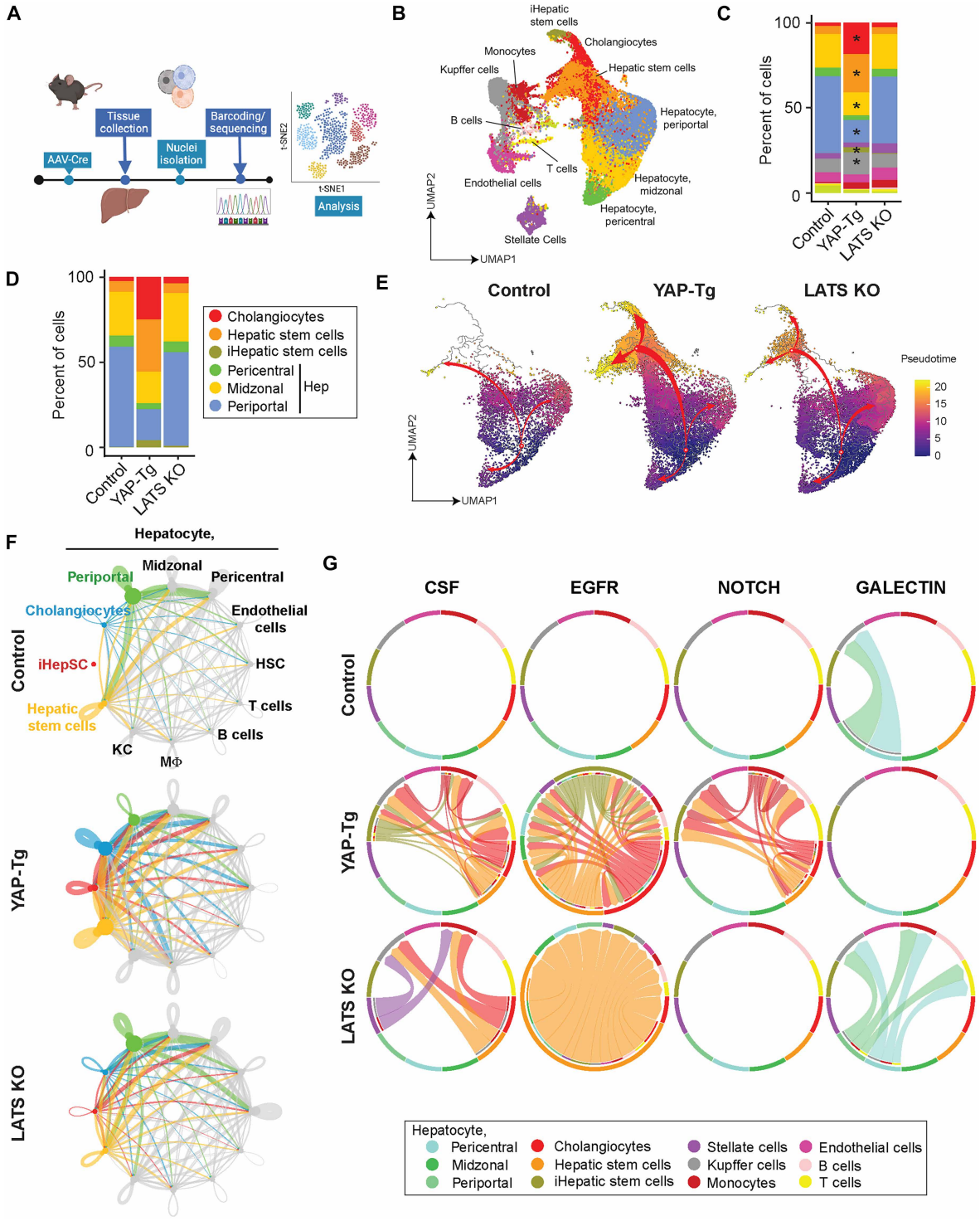

Fig. 3. Liver snRNA-seq demonstrates profound and novel interactions in YAP-Tg and LATS KO liver cell populations. (**A**) Schematic of experimental setup; nuclei were isolated from mouse livers at 0-, 1-, and 3-week time points and subjected to snRNA-seq. Created in BioRender. D. Yimlamai (2026), https://BioRender.com/2plsrsh. (**B**) Combined Uniform Manifold Approximation and Projection (UMAP) of 46,499 nuclei from control ($n = 2$, 5782 nuclei), YAP-Tg [1-week time point ($n = 2$) and 3-week time point ($n = 3$); total, 21,815 nuclei], and LATS KO [1-week time point ($n = 2$) and 3-week time point ($n = 2$); total, 18,902 nuclei] mice. Labels indicate identified cell types. (**C**) Proportion bar plot of UMAP cell populations in (A). Color scheme is maintained between (B) and (C). (**D**) Proportion bar plot of UMAP epithelial cell populations in (B) and (C). Color scheme is maintained between (C) and (D). (**E**) Monocle3 trajectory analysis plotted over UMAPs of control, YAP-Tg, and LATS KO conditions. Arrow width indicates relative strength of the trajectory analysis. (**F**) CellChat communication networks of all identified cell types across control, YAP-Tg, and LATS KO. Line thickness indicates the relative number of predicted interactions. (**G**) CellChat Interaction map of CSF, NOTCH, EGFR, and GALECTIN signaling in the indicated treatments. Cell types are indicated in the legend at the bottom.

Ly6c^{Hi} monocytes were enriched in both YAP-Tg (10.2%) and LATS KO (6.7%) livers as compared to controls (0.6%) but were preferentially present in YAP-Tg livers. Markers of T regulatory cell activity including *Foxp3*, *Ctla4*, *Il2ra*, and *Ikzf2* were enriched in LATS KO livers, supporting an anti-inflammatory environment in this context (fig. S3F).

Using CellChat (*43*), a machine learning algorithm coupled with a known ligand-receptor database, we evaluated potential cell-cell interactions in the context of these conditions. In YAP-Tg livers, most intercellular interactions originated from hepatic stem cells, iHepSCs, and cholangiocytes. These populations engage in extensive signaling with KCs, monocytic macrophages (Mϕ), and T and B cells. The intensity and frequency of these predicted interactions occurred at a higher rate in YAP-Tg livers than either the control or LATS KO conditions (Fig. 3F).

Several pathways identified by CellChat consistent with our phenotype included colony-stimulating factor 1 (*Csf1*) signaling, a well-characterized monocyte/macrophage chemotactic factor promoting their survival, proliferation, and differentiation (*44*, *45*). *Csf1* and its receptor, *Csf1r*, were absent in control livers, significantly enriched in YAP-Tg livers and moderately increased in LATS KO livers (Fig. 3G, CSF). *Egfr* and *Notch* signaling followed a similar trend as *Csf1*. These pathways are particularly salient with respect to the proinflammatory phenotype of YAP-Tg livers; *Egfr* is associated with macrophage recruitment and activation (*46*, *47*), whereas *Jag1-Notch2* signaling promotes a proinflammatory macrophage phenotype (*48*, *49*). Galectin signaling through *Lgals9* and *Cd44* was absent in YAP-Tg livers, present in controls, and enriched in LATS KO. Galectin signaling promotes immune tolerance and maintains hepatic homeostasis by balancing immune responses (*50*).

These analyses imply that hepatocytic YAP-Tg and LATS KO lead to similar levels of proliferation but differ in their ability to transdifferentiate affected cells. YAP-Tg influences hepatocytes to favor a more stem-like cell state as compared to LATS KO cells. In addition, YAP-Tg drives enhanced macrophage recruitment and inflammatory activation, whereas LATS KO cells are associated with anti-inflammatory immune signaling. Combined, these activities likely lead to the pruning of YAP-Tg cells by the immune system, despite similar proliferative levels between these two states.

Monocytes and T cells are rapidly recruited to YAP-Tg livers

To understand the complex spatial intercellular interactions intimated by the snRNA-seq analysis, we applied multiplexed error robust fluorescence in situ hybridization (MERFISH), a high-resolution spatial transcriptomics method that allows direct imaging of RNA species within their native tissue environment (*51*, *52*). Our probe set of 503 genes (table S2) was targeted to identify major cell types including cholangiocytes, hepatocytes, endothelial cells, fibroblasts, and immune cells. This approach enabled us to spatially resolve transcript distributions in the control and 1- and 4-week time points of YAP-Tg and LATS KO treatments (Fig. 4A and fig. S4A). We identified more than 2.19 million cells for analysis. We identified 12 transcriptionally distinct clusters that were validated against our snRNA-seq dataset using key marker genes (Fig. 4, A to C, and fig. S4B).

As anticipated, control livers exhibited normal architecture with clear zonation and minimal immune infiltration (Fig. 4A, control). Hepatocytes could be grouped into their major subtypes by expression of canonical marker genes: periportal (*Hal*, *Sds*, and *Cyp2r2*), midzonal (*Igfbp2*), and pericentral (*Oat*, *GluI*, and *Cyp2a5*). Hepatic stem cells were characterized by a mixture of periportal hepatocyte and cholangiocyte markers (*Sox9* and *Notch2*), without high gene expression representing cholangiocyte fate commitment (*Krt7* and *Krt19*). In controls, hepatic stem cells represented 0.5% of all cells. However, as early as 1 week postinduction, YAP-Tg livers were dominated by hepatic stem cells (54.2%) that were broadly distributed throughout the tissue and persisted at 4 weeks postinduction (37%; Fig. 4, A and D, YAP-Tg; and table S3). This seemed to come at the expense of all major hepatocyte sub-types as all these cell types were broadly reduced as compared to controls (Fig. 4D and table S3). Hepatic stem cells in LATS KO livers represented a small proportion of the liver as compared to YAP-Tg. They represented 0.6% of cells at 1 week and 5.6% at 4 weeks.

iHepSCs were identified by MERFISH in this dataset as well, although at a rate much lower than by snRNA-seq. These cells had the highest expression of *Ki67* of all cell types, akin to the snRNA-seq dataset. Our MERFISH probe set did not contain *Foxm1* that appears to be a characteristic marker for this cell type and may suggest that some hepatic stem cells are misclassified cells. Despite these caveats, iHepSCs were absent from controls, emerged in 1-week YAP-Tg livers (1.2%) and modestly increased at 4 weeks (2.1%). In contrast, iHepSCs were 0.1% at 1 week and 1.6% at 4 weeks in LATS KO livers.

With the distribution of these cells in mind, we questioned whether there were changes in the local cellular neighborhood composition between control, YAP-Tg, and LATS KO conditions. We applied a strategy that we previously described to examine local cellular neighborhood frequencies (*53*). Using the spatial coordinates of each labeled cell, we compute the frequency of a given cell type around a reference cell type of interest. These cell-type pairs allow us to detect changes between conditions at the neighborhood microscale and understand local dynamics potentially mediating cell-cell interactions (fig. S4C). The most profound shifts in cell-type associations occurred between the expanding epithelial populations and immune cells in the YAP-Tg and LATS KO conditions. We focused our subsequent analysis on the prospective epithelial-immune cell interactions (Fig. 4, D and E) to provide insights between the reference and neighboring cells in these conditions.

In controls, hepatic stem cells represented a rare population and infrequently colocalized with immune cell types of interest (0 to 7%). In YAP-Tg at 1 week, the frequency that monocytes associate with hepatic stem cells rose from 3% in controls to 44% ($P = 5.69 \times 10^{-35}$). At 4 weeks, they colocalize at 34% ($P = 5.89 \times 10^{-47}$). In LATS KO livers, these cells colocalize at comparatively lower frequencies (4% at 1 week and 17% at 4 weeks). When comparing between the YAP-Tg and LATS KO conditions, these cell types associate more frequently at 1 week ($P = 3.11 \times 10^{-45}$) and 4 weeks ($P = 0.00$) in the YAP-Tg condition.

Similar trends were observed when comparing the associations of other epithelial cell types that emerge in the YAP-Tg and LATS KO conditions (i.e., iHepSC and cholangiocytes) with immune cells (Fig. 4E). The most significant associations between immune cells to epithelial cells were highest in YAP-Tg livers, suggesting that YAP overexpression is consistent with relatively increased immune infiltration. The proximity of these immune cells to the hepatic stem cells, iHepSCs, and cholangiocytes implies a greater likelihood of cellular cross-talk supporting the snRNA-seq CellChat analysis.

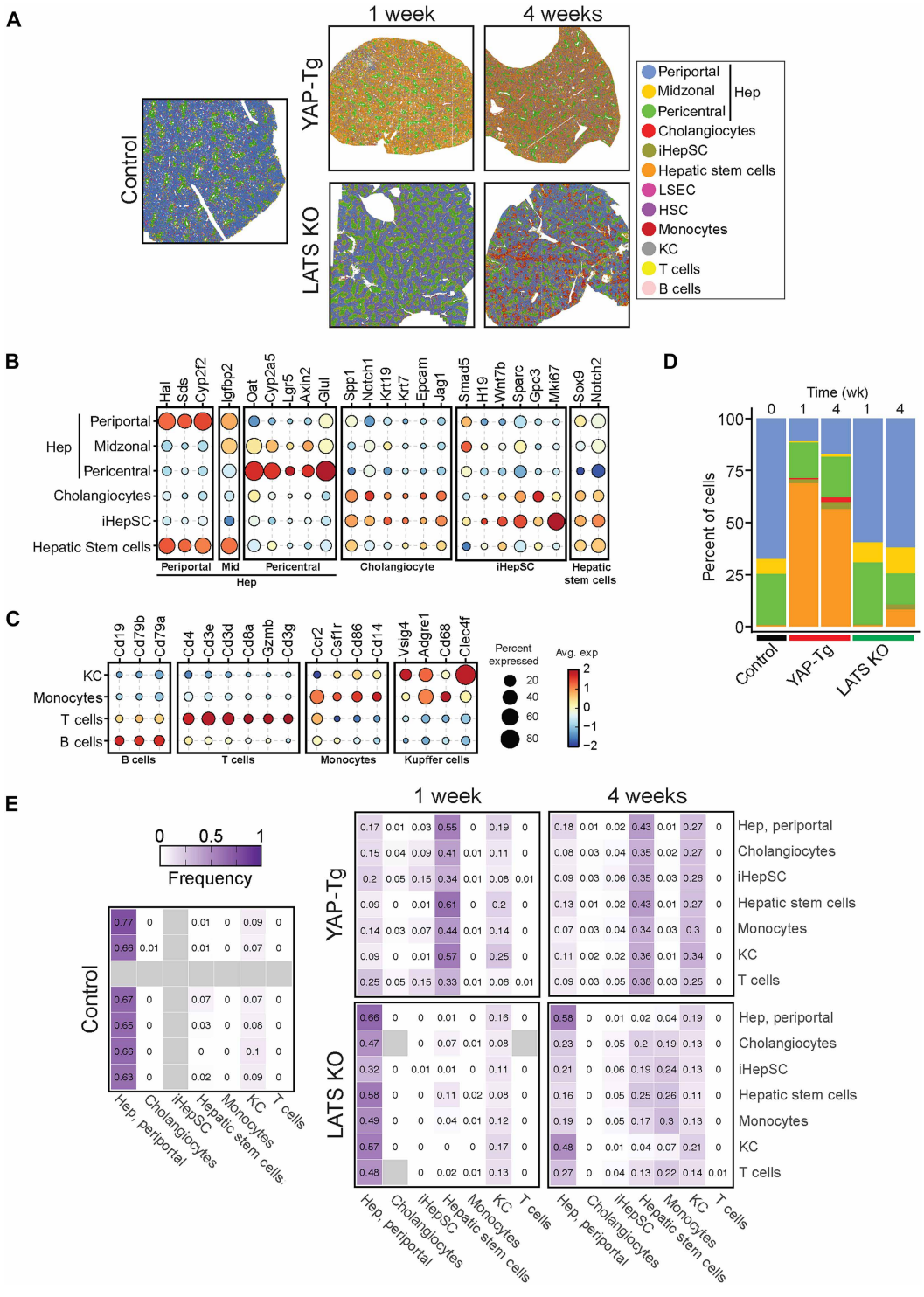

Fig. 4. MERFISH reveals changes to liver architecture in YAP-Tg model. (**A**) Images of control ($n = 1$), YAP-Tg [1 week ($n = 1$) and 4 weeks ($n = 1$)], and LATS KO [1 week ($n = 1$) and 4 weeks ($n = 1$)] livers postinduction with AAV-Cre (10^{11} PFU per mouse). Images are overlaid with cell-cluster labels. (**B**) Bubble plots display relative expression of marker genes used to identify epithelial cell populations. (**C**) Bubble plots display relative expression of marker genes used to identify selected immune cell populations. (**D**) Proportion bar plot of periportal, midzonal, pericentral hepatocytes (Hep); cholangiocytes; hepatic stem cells; and iHepSC. wk, weeks. (**E**) Heatmap representation of cell-type pair proximity frequency in control, YAP-Tg, and LATS KO livers; selected epithelial and immune cells. The number and the shading intensity are representative of increasing frequency of proximity.

YAP-Tg and LATS KO cells promote distinctive immune milieu associated with either cell elimination or immune suppression

Because immune cell recruitment and the interaction with YAP-Tg– and LATS KO–activated cells appeared to be critical to their long-term persistence, we isolated CD45$^+$ cells via FACS from either YAP-Tg ($n = 2$) or LATS KO ($n = 2$) livers 3 weeks after genetic activation. From these sorted immune cells, we generated scRNA-seq libraries for analysis (Fig. 5A). In this way, we captured a larger number of immune cells, and a higher proportion of cellular transcripts were identified from these cells, particularly cytoplasmic transcripts which are lost in snRNA-seq.

After filtering and clustering, we obtained 40,575 single cells from these two conditions for analysis. Twelve major cell clusters such as B, T, natural killer T (NKT) cells, neutrophils, monocytes, monocyte-derived KCs (MoKCs), and monocyte-derived macrophages (MoMacs) were identified through this process. A small but distinct highly-proliferative cell cluster was present in both settings that we labeled hematopoietic progenitors (*Cd34*^{Hi}*Gata2*^{Hi}*Cd34*^{Hi}). In this dataset, we did not identify KCs in either our YAP-Tg or LATS KO populations. The only identified clusters with well-accepted KC markers (i.e., *Clec4f*, *Timd4*, and *Vsig4*) also contained gene expression associated with monocyte recruitment (i.e., *Ccr2*, *Cx3cr1*, and *Ly6c2*) (*42*, *54*). Classical KC populations expressing only KC markers may exist within these livers, but they likely are masked within the large proportion of monocytes that are recruited to the YAP-Tg and LATKO livers and gradually adopt KC features. YAP-Tg livers demonstrated a larger proportion of T cells than LATS KO (28 versus 21.7%, respectively), particularly naïve T cells (11.8 versus 2.5%, respectively) (Fig. 5, B and C, and fig. S5A). Given that YAP-Tg livers recruit 35.5% more immune cells to the liver than LATS KO (fig. S3, C and D), this difference is particularly notable.

We then used CellChat to determine whether, within the YAP-Tg and LATS KO immune cells, there was significant cell-cell signaling that could support our hypothesis that YAP-Tg promotes proinflammatory signaling while LATS KO promotes an immune suppressive environment. Proinflammatory signaling was present in both conditions, but the frequency and complexity of potential cell-cell signaling within the YAP-Tg immune compartment for pathways such as tumor necrosis factor–α and interferon-γ were more prevalent. In contrast, potential interactions for *Cd80*/*Ctla4* immunosuppressive signaling occurred more frequently in the LATS KO livers (Fig. 5D).

From our spatial sequencing data, activated hepatocytes in both the YAP-Tg and LATS KO livers increase the frequency of their interaction with myeloid and T cells. To understand the potential shifts in these populations and their activity, we examined the myeloid and T cell compartments from the larger experiment, reclustering them to generate finer subdivisions from which to understand the complex dynamics within the livers of these animals. The myeloid dataset included 14,290 cells, divided into 14 clusters (Fig. 5, E and F, and fig. S5B). YAP-Tg livers demonstrated a larger proportion of neutrophil-1/-2 than LATS KO (46.3 versus 27.0%, respectively), clusters that express high *Il1β* and *Tnfα*. MoKC clusters were modestly enriched in the YAP-Tg condition (24.9 versus 20.7%), particularly MoKC1 (15.9 versus 0.7%). These clusters express high levels of complement (*C1qa*, *C1qb*, and *C1qc*), suggesting that they may be phagocytosing target cells (*55*, *56*). Gene set enrichment analysis (GSEA) of the MoKC1 population showed gene programs such as Cell Killing and CCR5 chemokine receptor binding to be favored in the YAP-Tg condition, while programs associated with Wound healing and metabolism were favored in LATS KO (fig. S6A).

The T cell subset contained 8413 cells forming 10 distinct clusters (Fig. 5, F and G, and fig. S5C) after reclustering. As mentioned earlier, naïve T cells dominated the YAP-Tg T cell population that was amplified after separation from the B and myeloid cell populations (34.9 versus 6.3%). Reclustering allowed identification of invariant NKT cells (iNKT) and Cd8 T effector cells that were not apparent in the larger immune dataset. YAP-Tg livers expressed a high proportion of the iNKT (27.3 versus 8.8%) and CD8 T effector (12.9 versus 4.7%) cells. These cell types are known to mediate cell death (*57*–*59*) with their increased prevalence in the YAP-Tg conditions, suggesting that it may play a role in their clearance. Using GSEA to annotate the gene sets associated with the iNKT2 and Cd8 T effector subsets, we identified programs such as immune recruitment, activation, and Regulation of Hepatocyte Apoptotic Process to be associated with YAP-Tg. Like the myeloid cell analysis, LATS KO was associated with metabolic gene sets and Positive Regulation of Hepatocyte Proliferation (fig. S6B). Together, YAP-Tg cells skew the immune milieu toward a proinflammatory environment primed toward mediating cell death.

CCR2-mediated inhibition promotes YAP-Tg clonal expansion

To explore the role of monocyte recruitment in the growth of YAP-predominant cells, we treated YAP-Tg mice with either a vehicle or CCR2 antagonist (CCR2i). CCR2 is well established in its role as a monocyte chemoattractant and is necessary for the recruitment of inflammatory monocytes/MoMacs from the blood to local tissue sites (*60*, *61*). YAP-Tg animals were injected with a single low-titer dose of AAV-TBG-Cre and given doxycycline-water for a period of 4 weeks to induce YAP overexpression in a small number of hepatocytes. Over the course of 4 weeks, animals were treated with a vehicle (control) or CCR2 inhibitor (CCR2i; Fig. 6A). Control and CCR2i livers did not significantly differ in gross morphology or percentage of liver/body weight (fig. S7, A and B). The macrophage marker F4/80 revealed an expected significant reduction in the CCR2i group with an average of 48.7 cells per HPF as compared to an average of 96.8 cells per HPF in controls (Fig. 6, B and C; $P < 0.01$). We then isolated liver immune cells from these livers and analyzed them by flow cytometry. We gated on liver macrophages (Live$^+$CD45$^+$Ly6G$^-$F4/80$^+$) and examined them for their activation status by the proportion of macrophages displaying Ly6c^{Hi}MHC^{low} (Fig. 6D) (*18*, *62*). There was a modest decrease in activated macrophages in the CCR2i-treated livers (Fig. 6E; 51.2 versus 38.6%, P = not significant) consistent with our prior findings. Microscopic examination of these livers revealed stark differences in the number of tdTomato$^+$ cells per field. In controls, there were 9.5 cells per HPF as compared to CCR2i with 60.2 cells per HPF (Fig. 5, D and E; $P < 0.05$). These findings implicate inflammatory monocyte recruitment as a negative regulator of YAP-Tg induced clonal growth and persistence.

TAZ^{High} cancers are associated with the shortest length of survival

Epithelial YAP- and TAZ-predominant clones evoke distinct immune responses in mice, causing preferential clearance of YAP clones. We then considered whether a similar phenomenon occurs in human

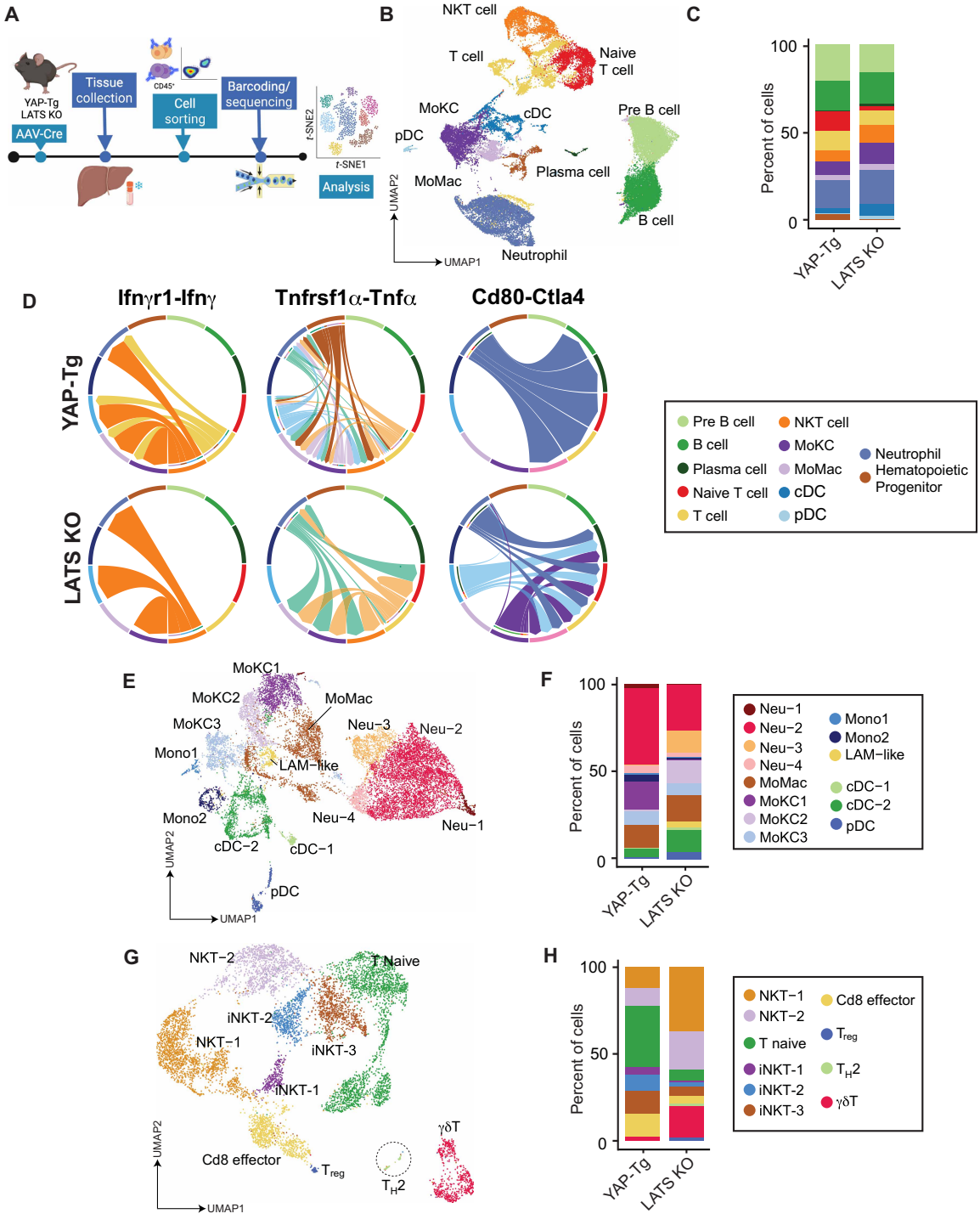

Fig. 5. scRNA-seq of the YAP-Tg and LATS KO liver immune compartment demonstrates distinctive sets of immune cell recruitment. (**A**) CD45$^+$ cells from 3 week activated YAP-Tg or LATS KO livers were isolated and subjected to scRNA-seq. Created in BioRender. D. Yimlamai (2026), https://BioRender.com/xuszqfe. (**B**) UMAP of 40,575 cells from YAP-Tg (n = 2, 24,737 cells) and LATS KO (n = 2, 15,838 cells) livers. Cluster colors are maintained between (B) and (D). (**C**) Bar Chart showing proportion of cells in the indicated treatments from (B). (**D**) CellChat Interaction map of *Ifnγ*, *Tnfα*, and *Ctla4* signaling in the indicated treatments. Cell types are indicated in the legend below. Arrows indicate the direction of signal and width indicates the relative magnitude of transcripts detected by scRNA-seq. (**E**) UMAP of myeloid subset showing 14,290 cells from YAP-Tg (n = 2, 7438 cells) and LATS KO (n = 2, 6842 cells). Cluster colors are maintained between (E) and (F). (**F**) Bar Chart showing proportion of cells in the indicated treatments from (E). (**G**) UMAP of T cell subset showing 8413 cells from YAP-Tg (n = 2, 5788 cells) and LATS KO (n = 2, 2625 cells). Cluster colors are maintained between (G) and (H). (**H**) Bar Chart showing proportion of cells in the indicated treatments from (G). T_H2, T helper 2.

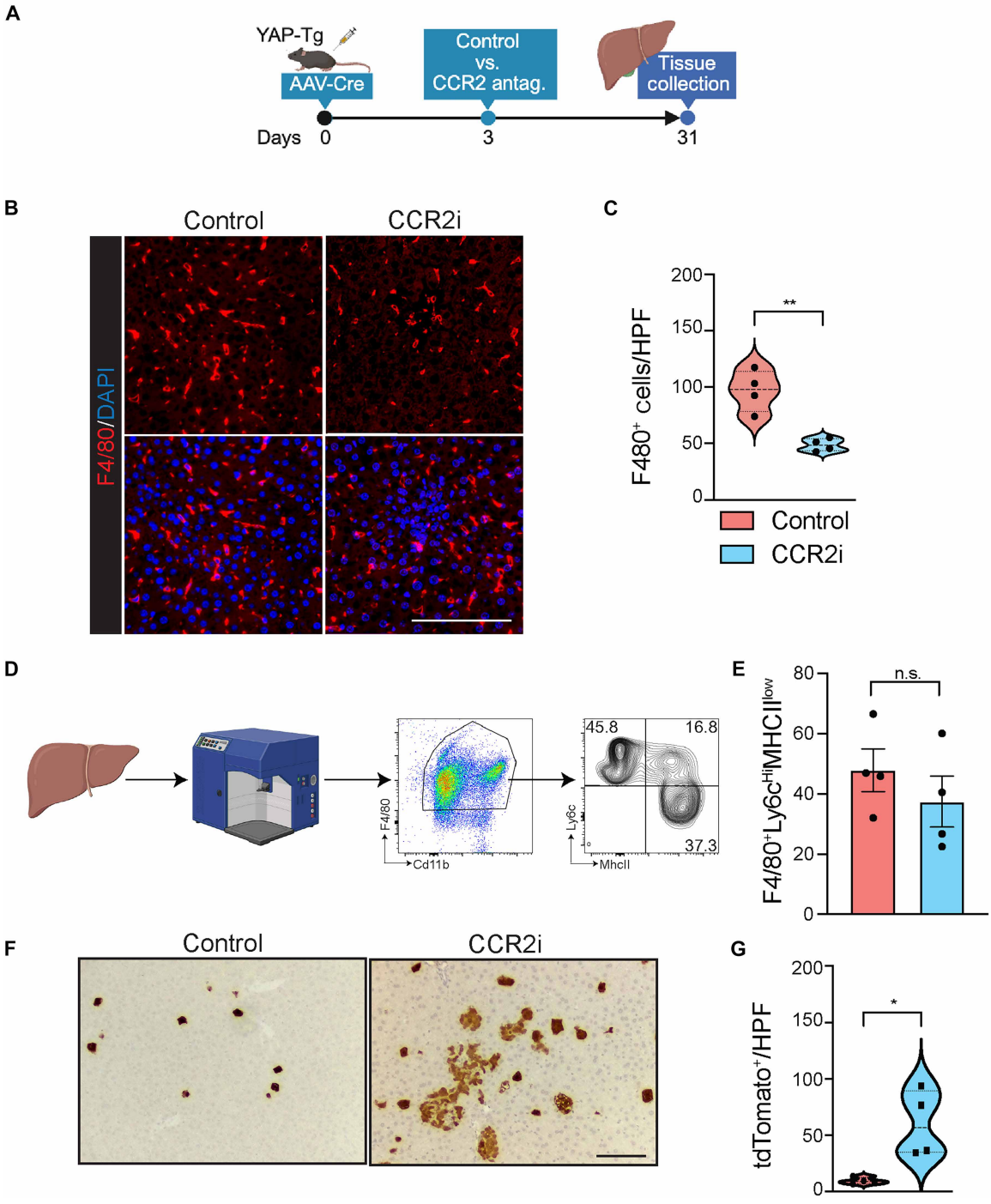

Fig. 6. Monocyte antagonism results in expanded YAP-Tg clone formation. (**A**) Schematic of experimental setup; YAP-Tg mice were treated with vehicle control or RS102895 (CCR2i) and harvested after 4 weeks. Created in BioRender. D. Yimlamai (2026), https://BioRender.com/dcwskw2. (**B**) Representative images of F4/80 immunostaining cells in the indicated conditions. Scale bar, 90 μm. (**C**) Violin plot of F4/80$^+$ cells per HPF for conditions noted in (B) ($n = 4$ animals per group; Student's unpaired t test). (**D**) Schematic of flow sorting and measurement of macrophages (F4/80$^+$) and their ratio of Ly6c and major histocompatibility complex (MHC) II expression. Partially created in Adobe Illustrator and BioRender. D. Yimlamai (2026), https://BioRender.com/elg0f3u. (**E**) Bar plot of F4/80$^+$Ly6c^{Hi}MHC^{low} expression from the indicated treatments. (**F**) Representative images of Red Fluorescent Protein immunostaining cells in the indicated conditions. Scale bar, 200 μm. (**G**) Violin plot of TdTomato$^+$ cells per HPF for conditions noted in (C) ($n = 4$ animals per group). n.s., not significant; *$P < 0.05$; **$P < 0.01$.

cancer and whether YAP or TAZ predominance leads to differences in patient outcomes. Using clinical patient information and their associated bulk RNA-seq data from The Cancer Genome Atlas (TCGA) (*63*, *64*), we stratified subjects into groups on the basis of their tumor's normalized relative expression of YAP and TAZ (top 30% or bottom 30%).

Patients with CRC were stratified into three groups: $YAP^{High}TAZ^{Low}$ (YAP^{High}), $YAP^{Low}TAZ^{High}$ (TAZ^{High}), and $YAP^{Low}TAZ^{Low}$ (YT^{Low}). Patients with YAP^{High} CRC had a 67% 5-year survival rate, whereas patients with TAZ^{High} CRC did not survive to 5 years. TAZ^{High} patients had a median survival time of 36.5 months. At 3 years, 100% of CRC YAP^{High} and YT^{Low} groups survived as compared to 58% of the TAZ^{High} CRC group ($P = 0.043$; Fig. 7A). Similar trends were observed in an HCC cohort. The survival probability of patients with TAZ^{High} HCC was 0% at 5 years but above 59% in both the YAP^{High} and YT^{Low} groups ($P = 0.38$; Fig. 7B).

We then investigated whether, in CRC, immune modulatory programs were present in the YAP^{High} and/or TAZ^{High} patient tumors as in our mouse models. GSEA using Gene Ontology (GO) pathways revealed that the YAP^{High} group was enriched for programs related to

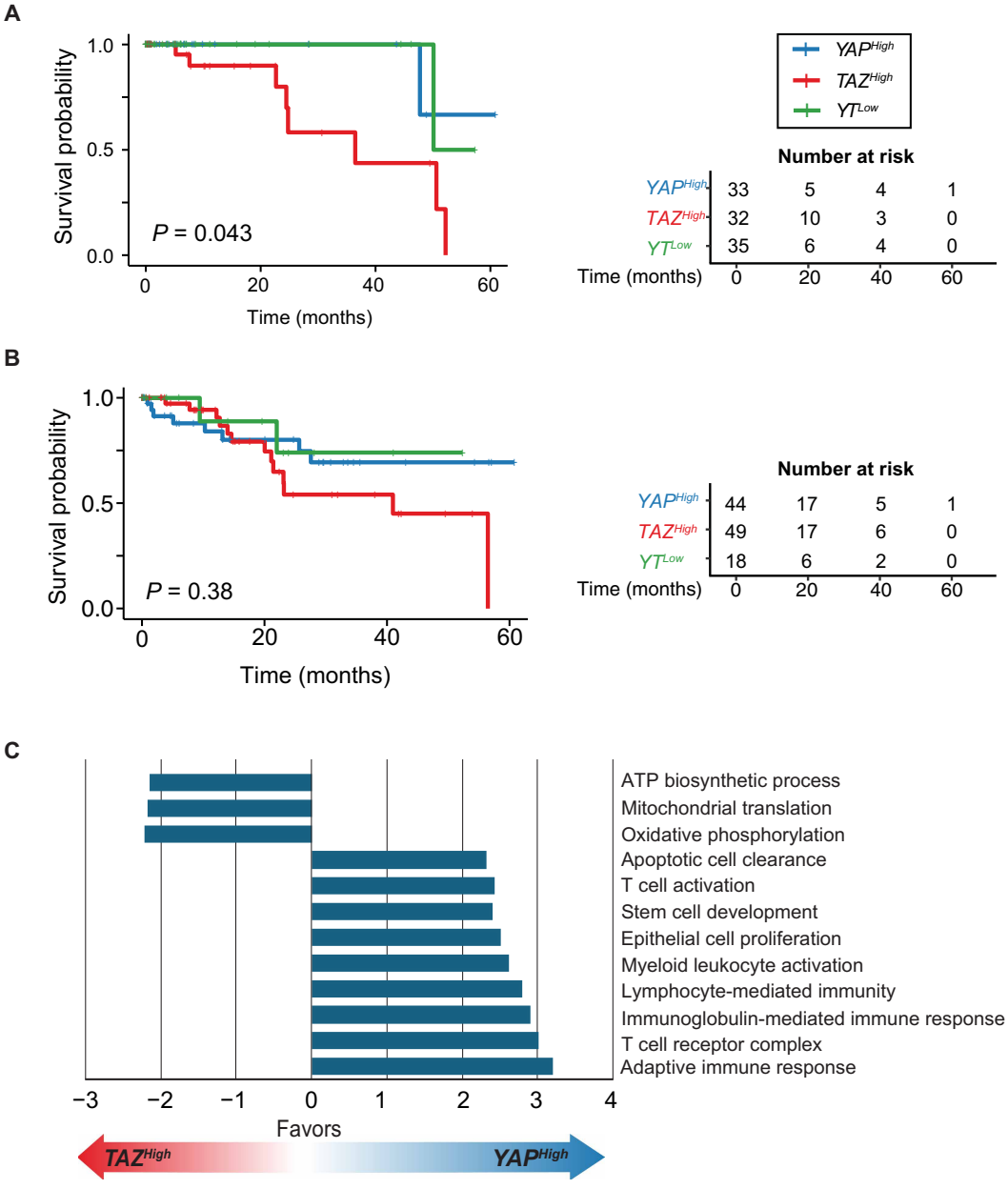

Fig. 7. High tumor YAP expression is correlated with immune activation and improved prognosis in CRC and HCC. (**A**) Kaplan-Meier survival plot of patients with CRC stratified into YAP^{High} ($n = 43$), TAZ^{High} ($n = 45$), and YT^{Low} ($n = 45$) groups. *P* value calculated by Kaplan-Meier log-rank test. (**B**) Kaplan-Meier survival plot of patients with HCC stratified into YAP^{High} ($n = 67$), TAZ^{High} ($n = 72$), and YT^{Low} ($n = 26$) groups. *P* value calculated by Kaplan-Meier log-rank test. (**C**) Gene Ontology (GO) pathway analysis; normalized enrichment score associated with the YAP^{High} or TAZ^{High} CRC groups. ATP, adenosine 5′-triphosphate.

cell death and immune stimulation such as apoptotic cell clearance, myeloid leukocyte activation, and T cell activation (Fig. 7C). This pattern was not mirrored in the TAZ^{High} group, which was enriched for pathways related to energy and cholesterol metabolism. Overall, these findings suggest that an immune-stimulatory gene expression program is associated with YAP^{High} cancers leading to comparatively improved patient survival to TAZ^{High} cancers.

DISCUSSION

The Hippo signaling pathway was originally discovered through genetic and biochemical screens to identify regulators of cell proliferation (*65*–*67*). Through this process, *yorkie* was revealed to act as a primary gatekeeper to the pathway. Genes are commonly duplicated through evolution, but preserving these genes in their original state is disadvantageous. Duplicated genes must diverge to assume new essential roles, justifying their maintenance. In vertebrates, *YAP* and *TAZ* emerged from *yorkie* (*3*) and are referred interchangeably, because they can be exchanged in many cellular assays. This perceived uniformity masks potentially important differences in the two.

Here, we combined targeted gene overexpression and lineage tracing with a multiomic approach to uncover nonredundant features of YAP and TAZ in vivo. Using the murine liver as a model, we up-regulated either YAP or TAZ in adult hepatocytes. The LATS KO used in this work is commonly accepted as a model for the effects of YAP/TAZ overexpression (*19*–*22*). Our discovery that, in the liver context, recombined LATS KO hepatocytes predominantly express TAZ and down-regulates YAP after 2 weeks was unexpected. Prior studies primarily focused on the initial proliferative burst that YAP/TAZ provide, so the possibility that YAP was absent at later time points may not have been fully appreciated. Recognizing that YAP is much larger than TAZ and contains several phosphorylation sites and domains not present on the other (*15*, *68*), it is easier to appreciate that these molecules may be regulated differently to serve distinct purposes. Whether this effect of LATS KO on YAP and TAZ expression is consistent in other contexts remains to be determined.

This work demonstrates that the TAZ-predominant clones produced by LATS KO result in a notable morphological growth phenotype that was not mirrored when we generated similar clones driven by YAP. Several mechanisms are at play in the development of these growth differences. First, YAP-predominant cells rapidly lose their hepatocyte identity, undergoing transcriptional reprogramming toward a stem-like fate characterized by the expression of markers of hepatobiliary stemness like *Sox9* and *Krt8*, in addition to up-regulation of *Foxm1*. *Foxm1* regulates genes involved in DNA replication and cellular proliferation, whereas its up-regulation in cancer has implicated it as a potential oncogene (*69*–*72*). This fate change was associated with the expression of many interferon-associated genes [i.e.,interferon regulatory factor 9 (*IRF9*), interferon-stimulated gene 15 (*ISG15*), and interferon-gamma-induced GTPase (*IGTP*)] that may be stimulating an antigrowth response and the production of several ligands (i.e., *Jag1*, *Csf1*, and *Egf*), which could recruit and activate blood-derived monocytes to the liver. The rise of this epithelial-stem compartment coincided with an expanded immune compartment and evidence of increased cell-cell communication with monocytes, KCs, and T cells.

In contrast, TAZ-predominant clones largely did not undergo a fate change and instead expressed genes associated with an immunosuppressive phenotype (i.e., *Ctla4* and *Tigit*). Classically, *Ctla4* is expressed in regulatory T cells (T_{reg} cells) and activated T cells to down-regulate immune responses (*25*). It is also found in tumor cells (*27*) where its secretion of a soluble *Ctla4* constrains T cells to noncytotoxic states (*69*–*72*). Likewise, intrinsic expression of *Tigit* by murine tumor cells promotes inhibitory natural killer and T cell signaling (*73*, *74*), a mechanism likely at play in TAZ-predominant cells. Supporting these findings was the expression of T_{reg} cell markers (i.e., *Foxp3*, *Il2ra*, and *Ctla-4*) within the broader T cell population in livers that overexpress nuclear TAZ. In addition, we observed up-regulation of effector T_{reg} cell markers (i.e., *Icos*, *Pd-1*, and *Cd44*), a transcriptional profile shown to infiltrate tumors and promote their growth (*75*).

Of the immune cells recruited by these models, we focused on monocytes and macrophages that are important in rewiring the cellular microenvironment (*76*–*78*). Both the YAP-Tg and LATS KO models are associated with increased immune infiltration, but the YAP-Tg model had an overall higher proportion of immune cell recruitment. Acute reduction in monocyte recruitment demonstrated a profound improvement in YAP-stimulated growth, supporting their role as a key brake limiting excessive cellular growth. Together, these findings suggest that recruited immune cells act in concert to limit YAP clonal expansion and support the notion that TAZ-predominating clonal expansion is aided by the development of an immunosuppressive microenvironment.

The mechanism by which common, YAP-, or TAZ-predominant targets are activated or inactivated remains a major unanswered question. Several portions of these molecules such as the TEAD binding and WW domains of these molecules are highly conserved, but other portions, such as the disordered portions of these molecules, show significant divergence (*15*, *68*). Proteins with disorganized regions such as YAP/TAZ are thought to participate in complementary protein-protein interactions to generate membraneless structures that organize biological functions. Also termed, bimolecular condensates or phase separation is a recently described mechanism to guide transcriptional specificity (*79*, *80*). Both YAP and TAZ have been reported to participate in this process (*81*, *82*). YAP and TAZ phase separate in the nuclei upon activation, such as changes in cell-cell contact. YAP-phase condensates include TAZ (*81*), but TAZ-phase condensates can exclude YAP (*82*). Understanding how this selectivity occurs and whether it drives the phenotypes described above is potentially a key strategy to advance regenerative/oncologic therapy.

Our finding that YAP and TAZ activation drives distinct immune environments in vivo and is associated with differential patient survival in YAP^{High} and TAZ^{High} cancers, suggests further investigation in the epithelial properties and the immunoreactivity these molecules stimulate should be examined more closely. We noted the presence of *Ctla4* and *Tigit* in the context of LATS KO. Would TAZ-predominant tumors respond to immune checkpoint molecules that target this or similar molecules? Is it beneficial in CRC or HCC to induce YAP expression when the expression of this molecule is low? Would it lead to an immunostimulatory environment leading to their clearance? Whether the findings that we describe here can be replicated in larger or independent cohorts remains to be examined.

There is significant interest in developing strategies to up-regulate YAP/TAZ activity (*83*) and target their downstream transcriptional activity (*84*–*86*). Now, these approaches target the common, well-ordered TEAD binding domain and are rapidly progressing through clinical trials. From this work, developing novel discriminating compounds for modulating YAP-TEAD or TAZ-TEAD activity may be an independent complementary therapeutic strategy for cancer.

MATERIALS AND METHODS

Mouse lines

C57BL/6J, *LATS1/2*$^{fl/fl}$ (*87*) (Jackson Laboratories, Bar Harbor, ME), and tetracycline-inducible *Yap-S127A* (TetOYAP/YAP-Tg) (*17*) were used in this study. Experiments were started at 8 to 12 weeks of age. Sequencing analysis was performed only with male mice. All mouse procedures and protocols were approved by Yale University's Institutional Animal Care and Use Committee under protocol no. 2023-20348.

AAV gene delivery, YAP overexpression, and LATS1/2 KO

Adeno-associated virus (AAV8)–thyroid hormone-binding globulin (TBG)–cyclization recombinase (Cre) (AAV-Cre; Addgene) was delivered to the indicated genotypes retro-orbitally at 10^{11} plaque-forming units (PFU) per mouse. To induce expression of TetOYAP, 3 days after AAV-Cre injections, mice were given doxycycline (1 mg/ml) ad libitum in drinking water. These mice are referred to as "YAP-Tg" in the text. To remove LATS1/2 from mice, a similar dose of AAV-Cre was given to *LATS1/2*$^{fl/fl}$ mice.

Tissue preparation, immunohistochemistry, and RNA in situ hybridization

Tissue was fixed overnight in 10% buffered formalin (Fisher Scientific) and embedded in paraffin for sectioning. For picrosirius red staining, tissue sections were rehydrated and incubated with 0.1% Direct Red (MilliporeSigma) and 0.08% Fast Green FCF (MilliporeSigma) in saturated picric acid (MilliporeSigma) for 1 hour. For immunohistochemistry, tissue sections were rehydrated and Citrate-based Unmasking Solution (Vector Labs) was used before staining. Images were taken with Revolve microscope (Echo).

RNA-seq analysis of previously published ApoE-YAP versus LATS KO

Data were downloaded from the Gene Expression Omnibus (GEO) under the accession number GSE211459 (liver, Yap hyperactivation). Raw count data were downloaded from the GEO supplementary file (GSE211459_YapHyper_Counts.txt.gz) and loaded into R. Gene level counts were extracted from the supplementary file. Experimental group labels (control, YAP-OE, LATS KO) were assigned to each of the samples based on information in the metadata. To improve data compatibility with downstream analysis tools, mouse gene symbols were converted to human orthologs using the convert_mouse_to_human_symbols() function from the nichenetr package (*88*). Any genes that could not be converted were excluded from further downstream analysis. For genes with duplicate symbols, the most variable symbol (based on interquartile range) was stored and used for further processing. The final cleaned expression matrix was converted to numeric values while gene symbols were set as row names. The voom transformation from the limma package (*89*) was used to normalize the data after creating a DGE-list with the edgeR package (*90*). The normalized data were then used for analysis to generate heatmaps and were further applied to IPA for enrichment analysis.

scRNA-seq library preparation and data analysis

Single lobes were isolated from mouse liver and snap frozen in liquid nitrogen. On the day of nuclei isolation, snap-frozen samples were gently split with a razor blade to yield small chunks of ~8 to 10 mm in diameter. Homogenization buffer (HB) was prepared as described (*91*). The sample was placed in a 1.5-ml tube with 750 μl of HB [0.1% Triton X-100, 1 μM dithiothreitol, 242.25 mM sucrose, 24.23 mM KCl, 4.85 mM $MgCl_2$, 9.69 mM tris (pH 8.0)] and then dounced five times with a loose pestle and 10 times with a tight pestle. The sample was then transferred to a fresh tube, and 250 μl of HB was added before incubation on ice for 5 min. The homogenized sample was then filtered through a 100-μm cell strainer (Corning). Filtrate was then passed through the 35-μm strainer cap of a polystyrene test tube (Corning). The sample was spun down at 500*g* for 5 min at 4°C. Density gradient purification was performed with OptiPrep Density Gradient Medium (Sigma-Aldrich).

Samples were fixed and permeabilized using the Parse Biosciences Evercode Fixation kit v2 according to the manufacturer's instructions. Samples were then stored at −80°C until needed for library preparation. Libraries were prepared using a Parse Biosciences Evercode Whole Transcriptome v2 barcoding kit according to the manufacturer's instructions as described in Evercode user manual v2.2.2. Libraries were sequenced at the Yale Center for Genome Analysis on the NovaSeqX, 100–base pair paired-end sequencing. Downstream statistical analyses were performed by R package Seurat. Nuclei with more than 400 genes expressed and less than 5000 count were regarded as valid nuclei for the downstream analysis. Normalization via SCTranfsorm, SCT integration, UMAP dimension reduction, and gene clustering/annotation analyses were performed on the valid cells. In addition, R package Monocle3 was applied to construct single-nucleus trajectories. On the basis of the Seurat processed data, a trajectory graph was inferred, and the single nuclei were ordered on a pseudo timescale.

Tissue processing, sample preparation, imaging, and data analysis for MERFISH

All MERFISH sample preparation was performed under ribonuclease (RNase)–free conditions. Frozen embedded livers were cryosectioned at 10-μm thickness at −16°C and mounted onto room temperature (RT) MERSCOPE beaded coverslips (Vizgen). After adherence, sections were refrozen for 5 to 15 min and then fixed in 4% paraformaldehyde (PFA) diluted in 1× phosphate-buffered saline (PBS) for 15 min. Sections were washed three times with 1× PBS for 5 min each and then stored in 70% ethanol (EtOH) overnight at 4°C to permeabilize the tissue. Sections were stored in 70% EtOH for a maximum of 3 weeks.

Sample preparation was performed using the sample prep kit (Vizgen) and Vizgen manufacturer's instructions for unfixed tissue. First, for cell boundary staining, sections were washed with 1× PBS, incubated in blocking solution (RNase inhibitor, New England Biolabs) in Cell Boundary Blocking Buffer Premix (Vizgen) for 1 hour at room temperature, incubated in primary staining solution (Cell Boundary Primary Staining Mix, Vizgen) in blocking solution for 1 hour at room temperature, washed three times with 1× PBS for 5 min each on a rocking platform, incubated in secondary staining solution [3:100 Cell Boundary Secondary Staining Mix (Vizgen) in blocking solution] for 1 hour at room temperature, washed three times with 1× PBS for 5 min each on a rocking platform, fixed in 4% PFA diluted in 1× PBS for 15 min, and washed two times with 1× PBS for 5 min, each. Next, sections were washed with the Sample Prep Wash Buffer (Vizgen), incubated in the Formamide Wash Buffer (Vizgen) for 30 min at 37°C, and then incubated in the gene panel mix for 42 to 46 hours at 37°C. Sections were then incubated two times in the Formamide Wash Buffer for 30 min each at 47°C and washed with sample prep wash buffer for at least 2 min. Sections were coated in gel embedding solution [0.05% w/v ammonium persulfate, 0.05% v/v

N,*N*,*N*′,*N*′-tetramethylethylenediamine in Gel Embedding Premix (Vizgen)] and incubated at RT for 1.5 hours, cleared in 1:5 concentration proteinase K in Clearing Premix (Vizgen) at 37°C, and then stored in 1:100 proteinase K in Clearing Premix at 37°C overnight or for a maximum of 7 days to clear lipids and proteins that may contribute to autofluorescence background noise.

Before imaging, sections were washed two times with the Sample Prep Wash Buffer, incubated in 4′,6-diamidino-2-phenylindole (DAPI) and PolyT Staining Reagent (Vizgen) for 15 min on a rocking platform, incubated in the Formamide Wash Buffer for 10 min, and washed again with the Sample Prep Wash Buffer.

Imaging was performed on the MERSCOPE platform (Vizgen) according to the manufacturer's instructions. Briefly, samples were loaded into the flow chamber of the instrument and the desired region for imaging was selected using a low-resolution mosaic of DAPI and Poly-T stains. Samples were then imaged at high resolution with a seven-plane *z*-stack and 1.5-μm spacing between adjacent *z*-planes to capture the entire 10-μm thickness of the tissue sections. Samples were then automatically imaged according to MERSCOPE imaging presets.

The average of the median volume was calculated across all the libraries, and the large cells with greater than three times of the average volume were filtered out. Next, the doublets were removed using tool Scrublet (*92*). Then, the processed data were further analyzed using Seurat (*93*). Per library, the gene-by-cell count matrix was normalized, followed by the reference mapping to the corresponding snRNA-seq dataset for cell annotation. Furthermore, the spatial cell-cell interaction analysis was performed using CellChat (*43*) and cell level proximity analysis (*53*). Briefly, we define a cell spatial neighborhood as the cells within five times the median distance of pairwise neighbor cells. As a result, per cell type, the proportions of interactions with all the other cell types were calculated.

Treatment of mice with CCR2 antagonist

Adult mice (6 to 8 weeks of age) were administered RS102895 (MedChemExpress) via oral gavage at a concentration of 10 mg/kg or the same volume of vehicle (25% dimethyl sulfoxide in drinking water) daily for 28 days. Mice were euthanized and livers were harvested/processed up to 24 hours after the final drug/vehicle administration.

Transcriptional analysis of TCGA patient survival data

TCGA data were retrieved using the RTCGA package (*94*). Samples were stratified by YAP/TAZ expression with the top 30% defined as high and the bottom 30% as low. Survival analysis and Kaplan-Meier plots were generated using the survival and survminer R package. The Kaplan-Meier log-rank test was used to compare the survival curves of the YAP^{High}, TAZ^{High}, and YT^{Low} groups. Differentially expressed genes were identified using DESeq2 (*95*), and GO pathway enrichment analysis was performed with clusterProfiler (*96*).

Supplementary Materials

This PDF file includes:

Supplementary Methods
Figs. S1 to S7
Tables S1 to S4
References

REFERENCES

1. J. A. Birchler, H. Yang, The multiple fates of gene duplications: Deletion, hypofunctionalization, subfunctionalization, neofunctionalization, dosage balance constraints, and neutral variation. *Plant Cell* **34**, 2466–2474 (2022).
2. S. Ohno, *Evolution by Gene Duplication* (Springer-Verlag, 1970).
3. J. E. Phillips, Y. Zheng, D. Pan, Assembling a Hippo: The evolutionary emergence of an animal developmental signaling pathway. *Trends Biochem. Sci.* **49**, 681–692 (2024).
4. H. Oh, K. D. Irvine, Yorkie: The final destination of Hippo signaling. *Trends Cell Biol.* **20**, 410–417 (2010).
5. J. H. Driskill, D. Pan, Control of stem cell renewal and fate by YAP and TAZ. *Nat. Rev. Mol. Cell Biol.* **24**, 895–911 (2023).
6. P. Guo, S. Wan, K. L. Guan, The Hippo pathway: Organ size control and beyond. *Pharmacol. Rev.* **77**, 100031 (2025).
7. J. R. Misra, K. D. Irvine, The Hippo signaling network and its biological functions. *Annu. Rev. Genet.* **52**, 65–87 (2018).
8. A. Sebe-Pedros, Y. Zheng, I. Ruiz-Trillo, D. Pan, Premetazoan origin of the hippo signaling pathway. *Cell Rep.* **1**, 13–20 (2012).
9. Y. Chen, H. Han, G. Seo, R. E. Vargas, B. Yang, K. Chuc, H. Zhao, W. Wang, Systematic analysis of the Hippo pathway organization and oncogenic alteration in evolution. *Sci. Rep.* **10**, 3173 (2020).
10. D. Hilman, U. Gat, The evolutionary history of YAP and the Hippo/YAP pathway. *Mol. Biol. Evol.* **28**, 2403–2417 (2011).
11. F. Kanai, P. A. Marignani, D. Sarbassova, R. Yagi, R. A. Hall, M. Donowitz, A. Hisaminato, T. Fujiwara, Y. Ito, L. C. Cantley, M. B. Yaffe, TAZ: A novel transcriptional co-activator regulated by interactions with 14-3-3 and PDZ domain proteins. *EMBO J.* **19**, 6778–6791 (2000).
12. R. Yagi, L. F. Chen, K. Shigesada, Y. Murakami, Y. Ito, A WW domain-containing yes-associated protein (YAP) is a novel transcriptional co-activator. *EMBO J.* **18**, 2551–2562 (1999).
13. B. Zhao, X. Ye, J. Yu, L. Li, W. Li, S. Li, J. Yu, J. D. Lin, C. Y. Wang, A. M. Chinnaiyan, Z. C. Lai, K. L. Guan, TEAD mediates YAP-dependent gene induction and growth control. *Genes Dev.* **22**, 1962–1971 (2008).
14. T. Oka, V. Mazack, M. Sudol, Mst2 and Lats kinases regulate apoptotic function of Yes kinase-associated protein (YAP). *J. Biol. Chem.* **283**, 27534–27546 (2008).
15. F. Reggiani, G. Gobbi, A. Ciarrocchi, V. Sancisi, YAP and TAZ are not identical twins. *Trends Biochem. Sci.* **46**, 154–168 (2021).
16. H. Y. K. Kaan, S. W. Chan, S. K. J. Tan, F. Guo, C. J. Lim, W. Hong, H. Song, Crystal structure of TAZ-TEAD complex reveals a distinct interaction mode from that of YAP-TEAD complex. *Sci. Rep.* **7**, 2035 (2017).
17. F. D. Camargo, S. Gokhale, J. B. Johnnidis, D. Fu, G. W. Bell, R. Jaenisch, T. R. Brummelkamp, YAP1 increases organ size and expands undifferentiated progenitor cells. *Curr. Biol.* **17**, 2054–2060 (2007).
18. D. Yimlamai, C. Christodoulou, G. G. Galli, K. Yanger, B. Pepe-Mooney, B. Gurung, K. Shrestha, P. Cahan, B. Z. Stanger, F. D. Camargo, Hippo pathway activity influences liver cell fate. *Cell* **157**, 1324–1338 (2014).
19. Y. Hao, A. Chun, K. Cheung, B. Rashidi, X. Yang, Tumor suppressor LATS1 is a negative regulator of oncogene YAP. *J. Biol. Chem.* **283**, 5496–5509 (2008).
20. J. Zhang, G. A. Smolen, D. A. Haber, Negative regulation of YAP by LATS1 underscores evolutionary conservation of the *Drosophila Hippo* pathway. *Cancer Res.* **68**, 2789–2794 (2008).
21. N. Nishioka, K. Inoue, K. Adachi, H. Kiyonari, M. Ota, A. Ralston, N. Yabuta, S. Hirahara, R. O. Stephenson, N. Ogonuki, R. Makita, H. Kurihara, E. M. Morin-Kensicki, H. Nojima, J. Rossant, K. Nakao, H. Niwa, H. Sasaki, The Hippo signaling pathway components Lats and Yap pattern Tead4 activity to distinguish mouse trophectoderm from inner cell mass. *Dev. Cell* **16**, 398–410 (2009).
22. Q.-Y. Lei, H. Zhang, B. Zhao, Z.-Y. Zha, F. Bai, X.-H. Pei, S. Zhao, Y. Xiong, K.-L. Guan, TAZ promotes cell proliferation and epithelial-mesenchymal transition and is inhibited by the Hippo pathway. *Mol. Cell. Biol.* **28**, 2426–2436 (2008).
23. J. Yi, L. Lu, K. Yanger, W. Wang, B. H. Sohn, B. Z. Stanger, M. Zhang, J. F. Martin, J. A. Ajani, J. Chen, J. S. Lee, S. Song, R. L. Johnson, Large tumor suppressor homologs 1 and 2 regulate mouse liver progenitor cell proliferation and maturation through antagonism of the coactivators YAP and TAZ. *Hepatology* **64**, 1757–1772 (2016).
24. I. M. Moya, S. A. Castaldo, L. Van den Mooter, S. Soheily, L. Sansores-Garcia, J. Jacobs, I. Mannaerts, J. Xie, E. Verboven, H. Hillen, A. Alguero-Nadal, R. Karaman, M. Van Haele, W. Kowalczyk, M. De Waegeneer, S. Verhulst, P. Karras, L. van Huffel, L. Zender, J. C. Marine, T. Roskams, R. Johnson, S. Aerts, L. A. van Grunsven, G. Halder, Peritumoral activation of the Hippo pathway effectors YAP and TAZ suppresses liver cancer in mice. *Science* **366**, 1029–1034 (2019).
25. W. Kowalczyk, L. Romanelli, M. Atkins, H. Hillen, C. Bravo Gonzalez-Blas, J. Jacobs, J. Xie, S. Soheily, E. Verboven, I. M. Moya, S. Verhulst, M. de Waegeneer, L. Sansores-Garcia, L. van Huffel, R. L. Johnson, L. A. van Grunsven, S. Aerts, G. Halder, Hippo signaling instructs ectopic but not normal organ growth. *Science* **378**, eabg3679 (2022).
26. A. W. Duncan, C. Dorrell, M. Grompe, Stem cells and liver regeneration. *Gastroenterology* **137**, 466–481 (2009).
27. Y. Saito, D. Yin, N. Kubota, X. Wang, A. Filliol, H. Remotti, A. Nair, L. Fazlollahi, Y. Hoshida, I. Tabas, K. J. Wangensteen, R. F. Schwabe, A therapeutically targetable TAZ-TEAD2

pathway drives the growth of hepatocellular carcinoma via ANLN and KIF23. *Gastroenterology* **164**, 1279–1292 (2023).
28. D. Oyewole-Said, V. Konduri, J. Vazquez-Perez, S. A. Weldon, J. M. Levitt, W. K. Decker, Beyond T-cells: Functional characterization of CTLA-4 expression in immune and non-immune cell types. *Front. Immunol.* **11**, 608024 (2020).
29. W. Ouyang, A. O'Garra, IL-10 family cytokines IL-10 and IL-22: From basic science to clinical translation. *Immunity* **50**, 871–891 (2019).
30. M. Saraiva, P. Vieira, A. O'Garra, Biology and therapeutic potential of interleukin-10. *J. Exp. Med.* **217**, e20190418 (2020).
31. J. Dong, G. Feldmann, J. Huang, S. Wu, N. Zhang, S. A. Comerford, M. F. Gayyed, R. A. Anders, A. Maitra, D. Pan, Elucidation of a universal size-control mechanism in *Drosophila* and mammals. *Cell* **130**, 1120–1133 (2007).
32. J. Burks, R. E. Reed, S. D. Desai, Free ISG15 triggers an antitumor immune response against breast cancer: A new perspective. *Oncotarget* **6**, 7221–7231 (2015).
33. J. Burks, R. E. Reed, S. D. Desai, ISGylation governs the oncogenic function of Ki-Ras in breast cancer. *Oncogene* **33**, 794–803 (2014).
34. M. Zhang, J. Li, H. Yan, J. Huang, F. Wang, T. Liu, L. Zeng, F. Zhou, ISGylation in innate antiviral immunity and pathogen defense responses: A review. *Front. Cell Dev. Biol.* **9**, 788410 (2021).
35. W. Xie, X. Gao, L. Zhao, S. Song, N. A. Li, J. Liu, *IRF9* and *STAT1* as biomarkers involved in T-cell immunity in atherosclerosis. *J. Biosci.* **49**, 84 (2024).
36. Y. Guan, X. Li, H. Yang, S. Xu, L. Shi, Y. Liu, L. Kong, Y. Qin, Role and mechanism of IRF9 in promoting the progression of rheumatoid arthritis by regulating macrophage polarization via PSMA5. *Heliyon* **10**, e35589 (2024).
37. M. Huber, T. Suprunenko, T. Ashhurst, F. Marbach, H. Raifer, S. Wolff, T. Strecker, B. Viengkhou, S. R. Jung, H. L. Obermann, S. Bauer, H. C. Xu, P. A. Lang, A. Tom, K. S. Lang, N. J. C. King, I. L. Campbell, M. J. Hofer, IRF9 prevents $CD8^+$ T cell exhaustion in an extrinsic manner during acute lymphocytic choriomeningitis virus infection. *J. Virol.* **91**, e01219-17 (2017).
38. A. Filliol, R. F. Schwabe, FoxM1 induces CCl2 secretion from hepatocytes triggering hepatic inflammation, injury, fibrosis, and liver cancer. *Cell. Mol. Gastroenterol. Hepatol.* **9**, 555–556 (2020).
39. C. Trapnell, D. Cacchiarelli, J. Grimsby, P. Pokharel, S. Li, M. Morse, N. J. Lennon, K. J. Livak, T. S. Mikkelsen, J. L. Rinn, The dynamics and regulators of cell fate decisions are revealed by pseudotemporal ordering of single cells. *Nat. Biotechnol.* **32**, 381–386 (2014).
40. J. Cao, M. Spielmann, X. Qiu, X. Huang, D. M. Ibrahim, A. J. Hill, F. Zhang, S. Mundlos, L. Christiansen, F. J. Steemers, C. Trapnell, J. Shendure, The single-cell transcriptional landscape of mammalian organogenesis. *Nature* **566**, 496–502 (2019).
41. W. Guo, Z. Li, G. Anagnostopoulos, W. T. Kong, S. Zhang, S. Chakarov, A. Shin, J. Qian, Y. Zhu, W. Bai, O. Cexus, B. Nie, J. Wang, X. Hu, C. Bleriot, Z. Liu, B. Shen, N. Venteclef, B. Su, F. Ginhoux, Notch signaling regulates macrophage-mediated inflammation in metabolic dysfunction-associated steatotic liver disease. *Immunity* **57**, 2310–2327.e6 (2024).
42. M. Guilliams, J. Bonnardel, B. Haest, B. Vanderborght, C. Wagner, A. Remmerie, A. Bujko, L. Martens, T. Thone, R. Browaeys, F. F. De Ponti, B. Vanneste, C. Zwicker, F. R. Svedberg, T. Vanhalewyn, A. Goncalves, S. Lippens, B. Devriendt, E. Cox, G. Ferrero, V. Wittamer, A. Willaert, S. J. F. Kaptein, J. Neyts, K. Dallmeier, P. Geldhof, S. Casaert, B. Deplancke, P. Ten Dijke, A. Hoorens, A. Vanlander, F. Berrevoet, Y. Van Nieuwenhove, Y. Saeys, W. Saelens, H. Van Vlierberghe, L. Devisscher, C. L. Scott, Spatial proteogenomics reveals distinct and evolutionarily conserved hepatic macrophage niches. *Cell* **185**, 379–396.e38 (2022).
43. S. Jin, M. V. Plikus, Q. Nie, CellChat for systematic analysis of cell-cell communication from single-cell transcriptomics. *Nat. Protoc.* **20**, 180–219 (2025).
44. A. Sehgal, K. M. Irvine, D. A. Hume, Functions of macrophage colony-stimulating factor (CSF1) in development, homeostasis, and tissue repair. *Semin. Immunol.* **54**, 101509 (2021).
45. C. V. Jones, S. D. Ricardo, Macrophages and CSF-1: Implications for development and beyond. *Organogenesis* **9**, 249–260 (2013).
46. D. M. Hardbower, K. Singh, M. Asim, T. G. Verriere, D. Olivares-Villagomez, D. P. Barry, M. M. Allaman, M. K. Washington, R. M. Peek Jr., M. B. Piazuelo, K. T. Wilson, EGFR regulates macrophage activation and function in bacterial infection. *J. Clin. Invest.* **126**, 3296–3312 (2016).
47. H. Lanaya, A. Natarajan, K. Komposch, L. Li, N. Amberg, L. Chen, S. K. Wculek, M. Hammer, R. Zenz, M. Peck-Radosavljevic, W. Sieghart, M. Trauner, H. Wang, M. Sibilia, EGFR has a tumour-promoting role in liver macrophages during hepatocellular carcinoma formation. *Nat. Cell Biol.* **16**, 972–981 (2014).
48. H. Xu, J. Zhu, S. Smith, J. Foldi, B. Zhao, A. Y. Chung, H. Outtz, J. Kitajewski, C. Shi, S. Weber, P. Saftig, Y. Li, K. Ozato, C. P. Blobel, L. B. Ivashkiv, X. Hu, Notch-RBP-J signaling regulates the transcription factor IRF8 to promote inflammatory macrophage polarization. *Nat. Immunol.* **13**, 642–650 (2012).
49. A. S. Kimball, A. D. Joshi, A. E. Boniakowski, M. Schaller, J. Chung, R. Allen, J. Bermick, W. F. Carson IV, P. K. Henke, I. Maillard, S. L. Kunkel, K. A. Gallagher, Notch regulates macrophage-mediated inflammation in diabetic wound healing. *Front. Immunol.* **8**, 635 (2017).
50. L. Golden-Mason, H. R. Rosen, Galectin-9: Diverse roles in hepatic immune homeostasis and inflammation. *Hepatology* **66**, 271–279 (2017).
51. K. H. Chen, A. N. Boettiger, J. R. Moffitt, S. Wang, X. Zhuang, RNA imaging. Spatially resolved, highly multiplexed RNA profiling in single cells. *Science* **348**, aaa6090 (2015).
52. J. R. Moffitt, J. Hao, G. Wang, K. H. Chen, H. P. Babcock, X. Zhuang, High-throughput single-cell gene-expression profiling with multiplexed error-robust fluorescence in situ hybridization. *Proc. Natl. Acad. Sci. U.S.A.* **113**, 11046–11051 (2016).
53. N. Tahmasian, M. Y. Feng, K. Arbabi, B. Rusu, W. Cao, B. Kukreja, A. Lubotzky, M. Wainberg, S. J. Tripathy, B. T. Kalish, Neonatal brain injury triggers niche-specific changes to cellular biogeography. *eNeuro* **11**, ENEURO.0224-24.2024 (2024).
54. S. A. Dick, A. Wong, H. Hamidzada, S. Nejat, R. Nechanitzky, S. Vohra, B. Mueller, R. Zaman, C. Kantores, L. Aronoff, A. Momen, D. Nechanitzky, W. Y. Li, P. Ramachandran, S. Q. Crome, B. Becher, M. I. Cybulsky, F. Billia, S. Keshavjee, S. Mital, C. S. Robbins, T. W. Mak, S. Epelman, Three tissue resident macrophage subsets coexist across organs with conserved origins and life cycles. *Sci. Immunol.* **7**, eabf7777 (2022).
55. S. Vandendriessche, M. S. Mattos, E. L. Bialek, S. Schuermans, P. Proost, P. E. Marques, Complement activation drives the phagocytosis of necrotic cell debris and resolution of liver injury. *Front. Immunol.* **15**, 1512470 (2024).
56. D. Feng, X. Xiang, Y. Guan, A. Guillot, H. Lu, C. Chang, Y. He, H. Wang, H. Pan, C. Ju, S. P. Colgan, F. Tacke, X. W. Wang, G. Kunos, B. Gao, Monocyte-derived macrophages orchestrate multiple cell-type interactions to repair necrotic liver lesions in disease models. *J. Clin. Invest.* **133**, e166954 (2023).
57. M. Bedard, M. Salio, V. Cerundolo, Harnessing the power of invariant natural killer T cells in cancer immunotherapy. *Front. Immunol.* **8**, 1829 (2017).
58. S. Arora, P. J. Thompson, Y. Wang, A. Bhattacharyya, H. Apostolopoulou, R. Hatano, R. P. Naikawadi, A. Shah, P. J. Wolters, S. Koliwad, M. Bhattacharya, A. Bhushan, Invariant natural killer T cells coordinate removal of senescent cells. *Med* **2**, 938–950.e8 (2021).
59. B. Farhood, M. Najafi, K. Mortezaee, $CD8^+$ cytotoxic T lymphocytes in cancer immunotherapy: A review. *J. Cell. Physiol.* **234**, 8509–8521 (2019).
60. L. Boring, J. Gosling, S. W. Chensue, S. L. Kunkel, R. V. Farese Jr., H. E. Broxmeyer, I. F. Charo, Impaired monocyte migration and reduced type 1 (Th1) cytokine responses in C-C chemokine receptor 2 knockout mice. *J. Clin. Invest.* **100**, 2552–2561 (1997).
61. C. L. Tsou, W. Peters, Y. Si, S. Slaymaker, A. M. Aslanian, S. P. Weisberg, M. Mack, I. F. Charo, Critical roles for CCR2 and MCP-3 in monocyte mobilization from bone marrow and recruitment to inflammatory sites. *J. Clin. Invest.* **117**, 902–909 (2007).
62. D. S. Shouval, A. Biswas, J. A. Goettel, K. McCann, E. Conaway, N. S. Redhu, I. D. Mascanfroni, Z. Al Adham, S. Lavoie, M. Ibourk, D. D. Nguyen, J. N. Samsom, J. C. Escher, R. Somech, B. Weiss, R. Beier, L. S. Conklin, C. L. Ebens, F. G. Santos, A. R. Ferreira, M. Sherlock, A. K. Bhan, W. Muller, J. R. Mora, F. J. Quintana, C. Klein, A. M. Muise, B. H. Horwitz, S. B. Snapper, Interleukin-10 receptor signaling in innate immune cells regulates mucosal immune tolerance and anti-inflammatory macrophage function. *Immunity* **40**, 706–719 (2014).
63. Cancer Genome Atlas Research Network, J. N. Weinstein, E. A. Collisson, G. B. Mills, K. R. Shaw, B. A. Ozenberger, K. Ellrott, I. Shmulevich, C. Sander, J. M. Stuart, The Cancer Genome Atlas Pan-Cancer analysis project. *Nat. Genet.* **45**, 1113–1120 (2013).
64. N. T. Nguyen, R. T. Cotton, T. R. Harring, J. J. Guiteau, M. C. Gingras, D. A. Wheeler, C. A. O'Mahony, R. A. Gibbs, F. C. Brunicardi, J. A. Goss, A primer on a hepatocellular carcinoma bioresource bank using the cancer genome atlas guidelines: Practical issues and pitfalls. *World J. Surg.* **35**, 1732–1737 (2011).
65. D. Pan, The unfolding of the Hippo signaling pathway. *Dev. Biol.* **487**, 1–9 (2022).
66. K. D. Irvine, K. F. Harvey, Control of organ growth by patterning and Hippo signaling in *Drosophila*. *Cold Spring Harb. Perspect. Biol.* **7**, (2015), 10.1101/cshperspect.a019224.
67. Z. M. S. Ma, R. Chen, K.-L. Guan, The Hippo pathway: Biology and pathophysiology. *Annu. Rev. Biochem.* **88**, 577–604 (2019).
68. S. Piccolo, S. Dupont, M. Cordenonsi, The biology of YAP/TAZ: Hippo signaling and beyond. *Physiol. Rev.* **94**, 1287–1312 (2014).
69. F. Xie, X. Zhou, Y. Ran, R. Li, J. Zou, S. Wan, P. Su, X. Meng, H. Yan, H. Lu, H. Ru, H. Hu, Z. Mao, B. Yang, F. Zhou, L. Zhang, Targeting FOXM1 condensates reduces breast tumour growth and metastasis. *Nature* **638**, 1112–1121 (2025).
70. S. Raghuwanshi, X. Zhang, Z. Arbieva, I. Khan, H. Mohammed, Z. Wang, A. Domling, C. J. Camacho, A. L. Gartel, Novel FOXM1 inhibitor STL001 sensitizes human cancers to a broad-spectrum of cancer therapies. *Cell Death Discov.* **10**, 211 (2024).
71. G. B. Liao, X. Z. Li, S. Zeng, C. Liu, S. M. Yang, L. Yang, C. J. Hu, J. Y. Bai, Regulation of the master regulator FOXM1 in cancer. *Cell Commun. Signal* **16**, 57 (2018).
72. I. Wierstra, FOXM1 (Forkhead box M1) in tumorigenesis: Overexpression in human cancer, implication in tumorigenesis, oncogenic functions, tumor-suppressive properties, and target of anticancer therapy. *Adv. Cancer Res.* **119**, 191–419 (2013).
73. X.-M. Zhou, W.-Q. Li, Y.-H. Wu, L. Han, X.-G. Cao, X.-M. Yang, H.-F. Wang, W.-S. Zhao, W.-J. Zhai, Y.-M. Qi, Y.-F. Gao, Intrinsic expression of immune checkpoint molecule TIGIT could help tumor growth *in vivo* by suppressing the function of NK and $CD8^+$ T cells. *Front. Immunol.* **9**, 2821 (2018).
74. H. Yu, S. Jin, M. Zeng, Z. Yang, X. Wang, TIGIT antibody with PVR competitive ability enhances cancer immunotherapy and capable of eliciting anti-tumour immune memory. *Br. J. Cancer* **133**, 743–755 (2025).

75. T. Wertheimer, P. Zwicky, L. Rindlisbacher, C. Sparano, M. Vermeer, B. M. S. de Melo, C. Haftmann, T. Ruckert, A. Sethi, S. Scharli, A. Huber, F. Ingelfinger, C. Xu, D. Kim, P. Hane, A. Fonseca da Silva, A. Muschaweckh, N. Nunez, S. Krishnarajah, N. Kohler, R. Zeiser, M. Oukka, T. Korn, S. Tugues, B. Becher, IL-23 stabilizes an effector T_{reg} cell program in the tumor microenvironment. *Nat. Immunol.* **25**, 512–524 (2024).
76. M. Mooring, B. H. Fowl, S. Z. C. Lum, Y. Liu, K. Yao, S. Softic, R. Kirchner, A. Bernstein, A. D. Singhi, D. G. Jay, C. R. Kahn, F. D. Camargo, D. Yimlamai, Hepatocyte stress increases expression of Yes-associated protein and transcriptional coactivator with PDZ-binding motif in hepatocytes to promote parenchymal inflammation and fibrosis. *Hepatology* **71**, 1813–1830 (2020).
77. M. Mooring, G. A. Yeung, P. Luukkonen, S. Liu, M. W. Akbar, G. J. Zhang, O. Balogun, X. Yu, R. Mo, K. Nejak-Bowen, M. V. Poyurovsky, C. J. Booth, L. Konnikova, G. I. Shulman, D. Yimlamai, Hepatocyte CYR61 polarizes profibrotic macrophages to orchestrate NASH fibrosis. *Sci. Transl. Med.* **15**, eade3157 (2023).
78. W. Kim, S. K. Khan, Y. Liu, R. Xu, O. Park, Y. He, B. Cha, B. Gao, Y. Yang, Hepatic Hippo signaling inhibits protumoural microenvironment to suppress hepatocellular carcinoma. *Gut* **67**, 1692–1703 (2018).
79. B. Wang, L. Zhang, T. Dai, Z. Qin, H. Lu, L. Zhang, F. Zhou, Liquid-liquid phase separation in human health and diseases. *Signal Transduct. Target. Ther.* **6**, 290 (2021).
80. D. Hnisz, K. Shrinivas, R. A. Young, A. K. Chakraborty, P. A. Sharp, A phase separation model for transcriptional control. *Cell* **169**, 13–23 (2017).
81. D. Cai, D. Feliciano, P. Dong, E. Flores, M. Gruebele, N. Porat-Shliom, S. Sukenik, Z. Liu, J. Lippincott-Schwartz, Phase separation of YAP reorganizes genome topology for long-term YAP target gene expression. *Nat. Cell Biol.* **21**, 1578–1589 (2019).
82. Y. Lu, T. Wu, O. Gutman, H. Lu, Q. Zhou, Y. I. Henis, K. Luo, Phase separation of TAZ compartmentalizes the transcription machinery to promote gene expression. *Nat. Cell Biol.* **22**, 453–464 (2020).
83. K. Namoto, C. Baader, V. Orsini, A. Landshammer, E. Breuer, K. T. Dinh, R. Ungricht, M. Pikiolek, S. Laurent, B. Lu, A. Aebi, K. Schonberger, E. Vangrevelinghe, O. Evrova, T. Sun, S. Annunziato, J. Lachal, E. Redmond, L. Wang, K. Wetzel, P. Capodieci, J. Turner, G. Schutzius, V. Unterreiner, M. Trunzer, N. Buschmann, D. Behnke, R. Machauer, C. Scheufler, C. N. Parker, M. Ferro, A. Grevot, A. Beyerbach, W. Y. Lu, S. J. Forbes, J. Wagner, T. Bouwmeester, J. Liu, B. Sohal, S. Sahambi, L. E. Greenbaum, F. Lohmann, P. Hoppe, F. Cong, A. W. Sailer, H. Ruffner, R. Glatthar, B. Humar, P. A. Clavien, M. T. Dill, E. George, J. Maibaum, P. Liberali, J. S. Tchorz, NIBR-LTSi is a selective LATS kinase inhibitor activating YAP signaling and expanding tissue stem cells in vitro and in vivo. *Cell Stem Cell* **31**, 554–569.e17 (2024).
84. T. T. Tang, A. W. Konradi, Y. Feng, X. Peng, M. Ma, J. Li, F. X. Yu, K. L. Guan, L. Post, Small molecule inhibitors of TEAD auto-palmitoylation selectively inhibit proliferation and tumor growth of NF2-deficient mesothelioma. *Mol. Cancer Ther.* **20**, 986–998 (2021).
85. Y. Liu-Chittenden, B. Huang, J. S. Shim, Q. Chen, S. J. Lee, R. A. Anders, J. O. Liu, D. Pan, Genetic and pharmacological disruption of the TEAD-YAP complex suppresses the oncogenic activity of YAP. *Genes Dev.* **26**, 1300–1305 (2012).
86. E. A. Chapeau, L. Sansregret, G. G. Galli, P. Chene, M. Wartmann, T. P. Mourikis, P. Jaaks, S. Baltschukat, I. A. M. Barbosa, D. Bauer, S. M. Brachmann, C. Delaunay, C. Estadieu, J. E. Faris, P. Furet, S. Harlfinger, A. Hueber, E. Jimenez Nunez, D. P. Kodack, E. Mandon, T. Martin, Y. Mesrouze, V. Romanet, C. Scheufler, H. Sellner, C. Stamm, D. Sterker, L. Tordella, F. Hofmann, N. Soldermann, T. Schmelzle, Author Correction: Direct and selective pharmacological disruption of the YAP-TEAD interface by IAG933 inhibits Hippo-dependent and RAS-MAPK-altered cancers. *Nat. Cancer* **5**, 1130 (2024).
87. Q. Chen, N. Zhang, R. Xie, W. Wang, J. Cai, K. S. Choi, K. K. David, B. Huang, N. Yabuta, H. Nojima, R. A. Anders, D. Pan, Homeostatic control of Hippo signaling activity revealed by an endogenous activating mutation in YAP. *Genes Dev.* **29**, 1285–1297 (2015).
88. R. Browaeys, W. Saelens, Y. Saeys, NicheNet: Modeling intercellular communication by linking ligands to target genes. *Nat. Methods* **17**, 159–162 (2020).
89. M. E. Ritchie, B. Phipson, D. Wu, Y. Hu, C. W. Law, W. Shi, G. K. Smyth, limma powers differential expression analyses for RNA-sequencing and microarray studies. *Nucleic Acids Res.* **43**, e47 (2015).
90. M. D. Robinson, D. J. McCarthy, G. K. Smyth, edgeR: A Bioconductor package for differential expression analysis of digital gene expression data. *Bioinformatics* **26**, 139–140 (2010).
91. E. R. Nadelmann, J. M. Gorham, D. Reichart, D. M. Delaughter, H. Wakimoto, E. L. Lindberg, M. Litvinukova, H. Maatz, J. J. Curran, D. Ischiu Gutierrez, N. Hubner, C. E. Seidman, J. G. Seidman, Isolation of nuclei from mammalian cells and tissues for single-nucleus molecular profiling. *Curr. Protoc.* **1**, e132 (2021).
92. S. L. Wolock, R. Lopez, A. M. Klein, Scrublet: Computational identification of cell doublets in single-cell transcriptomic data. *Cell Syst.* **8**, 281–291.e9 (2019).
93. Y. Hao, T. Stuart, M. H. Kowalski, S. Choudhary, P. Hoffman, A. Hartman, A. Srivastava, G. Molla, S. Madad, C. Fernandez-Granda, R. Satija, Dictionary learning for integrative, multimodal and scalable single-cell analysis. *Nat. Biotechnol.* **42**, 293–304 (2024).
94. M. Kosinski, P. Biecek, W. Chodor, The family of R packages containing TCGA data, v1.27.2, Github (2025); http://rtcga.github.io/RTCGA.
95. M. I. Love, W. Huber, S. Anders, Moderated estimation of fold change and dispersion for RNA-seq data with DESeq2. *Genome Biol.* **15**, 550 (2014).
96. T. Wu, E. Hu, S. Xu, M. Chen, P. Guo, Z. Dai, T. Feng, L. Zhou, W. Tang, L. Zhan, X. Fu, S. Liu, X. Bo, G. Yu, clusterProfiler 4.0: A universal enrichment tool for interpreting omics data. *Innovation* **2**, 100141 (2021).
97. A. M. Bolger, M. Lohse, B. Usadel, Trimmomatic: A flexible trimmer for Illumina sequence data. *Bioinformatics* **30**, 2114–2120 (2014).
98. A. Dobin, C. A. Davis, F. Schlesinger, J. Drenkow, C. Zaleski, S. Jha, P. Batut, M. Chaisson, T. R. Gingeras, STAR: Ultrafast universal RNA-seq aligner. *Bioinformatics* **29**, 15–21 (2013).
99. A. Subramanian, P. Tamayo, V. K. Mootha, S. Mukherjee, B. L. Ebert, M. A. Gillette, A. Paulovich, S. L. Pomeroy, T. R. Golub, E. S. Lander, J. P. Mesirov, Gene set enrichment analysis: A knowledge-based approach for interpreting genome-wide expression profiles. *Proc. Natl. Acad. Sci. U.S.A.* **102**, 15545–15550 (2005).

Acknowledgments: We thank Keck Microarray Shared Resource (KMSR) at Yale University for the assistance with 10x Genomics RNA-seq library preparation, the Yale Center for Genome Analysis for next-generation sequencing services, and M. Akbar for technical assistance preparing mouse samples. Graphic illustrations are created using BioRender.com through the Yale University Institutional license. **Funding:** This work was supported by the National Institutes of Health, grants R01DK129552 (D.Y.), R35 GM159862 (S.L.), P30 DK120531 (Pittsburgh Liver Research Center), P30 DK034989 (Yale Liver Center), S10 OD030363-01A1 (Yale Center for Genome Analysis), and P30 CA016359 (Yale Flow Cytometry Shared Resource).
Author contributions: Conceptualization: S.S. and D.Y. Methodology: S.S., S.L., N.T., and J.-J.L. Formal analysis: D.Y., J.-J.L., S.S., and S.L. Funding acquisition: D.Y. and S.L. Data curation: S.S. and S.L. Investigation: B.T.K., D.Y., J.-J.L., L.H., S.S., and S.L. Methodology: B.T.K. and D.Y. Project administration: D.Y. and S.S. Resources: D.Y. Software: B.T.K., D.Y., S.S., and S.L. Supervision: B.T.K., S.L., and D.Y. Validation: D.Y. and S.S. Visualization: D.Y., J.-J.L., S.S., and S.L. Writing—original draft: S.S., S.L., and D.Y. Writing—review and editing: B.T.K., L.H., S.S., S.L., and D.Y. All authors provided intellectual input, vetted, and approved the final manuscript. **Competing interests:** The authors declare that they have no competing interests. **Data, code, and materials availability:** The bulk RNA-seq, snRNA-seq, scRNA-seq, and spatial transcriptomics data have been deposited in the GEO database with accession ID GSE314329. All data and code needed to evaluate and reproduce the results in the paper are present in the paper and/or the Supplementary Materials. This study did not generate new materials.

Submitted 17 December 2025
Accepted 12 May 2026
Published 24 June 2026
10.1126/sciadv.aee8580